Geological Society of America Bulletin, published online on 2 September 2015 as doi:10.1130/B31341.1

Structure and evolution of volcanic plumbing systems in fold-and-thrust belts: A case study of the Cerro Negro de Tricao Malal, Neuquén Province, Argentina

Derya Gürer[1,†], Olivier Galland[1], Fernando Corfu[2], Héctor A. Leanza[3], and Caroline Sassier[4]

[1]*Physics of Geological Processes (PGP), Department of Geosciences, University of Oslo, P.O. Box 1048, Blindern, 0316 Oslo, Norway*

[2]*Department of Geosciences & Centre for Earth Evolution and Dynamics (CEED), University of Oslo, P.O. Box 1047, Blindern, 0316 Oslo, Norway*

[3]*Museo Argentino de Ciencias Naturales–Consejo Nacional de Investigaciones Científicas y Técnicas (CONICET), Avenida Angel Gallardo 470, 1405 Buenos Aires, Argentina*

[4]*Department of Geosciences, University of Oslo, P.O. Box 1047, Blindern, 0316 Oslo, Norway*

ABSTRACT

Magma ascent and emplacement in compressional tectonic settings remain poorly understood. Geophysical studies show that volcanic plumbing systems in compressional environments are vertically partitioned into a deep level subject to regional compression and a shallow level subject to local extension. Such vertical partitioning has also been documented for the plumbing systems of mud volcanoes, implying common, yet unresolved, underlying processes. In order to better constrain the mechanisms governing this depth partitioning of emplacement mechanisms, we studied the structure and evolution of the Cerro Negro intrusive complex emplaced in the Chos Malal fold-and-thrust belt in the foothills of the Neuquén Andes, Argentina. The Cerro Negro intrusive complex consists of sills and N-S–striking dikes that crosscut the sills. The most prominent structures in the study area are N-S–trending folds, and both E- and W-vergent thrusts. We provide new U-Pb ages of 11.63 ± 0.20 Ma and 11.58 ± 0.18 Ma for sills and 11.55 ± 0.06 Ma for a dike, which show that the Cerro Negro intrusive complex was emplaced in a short period of time. Our ages and field observations demonstrate that the emplacement of the Cerro Negro intrusive complex was coeval with the tectonic development of the Chos Malal fold-and-thrust belt. This implies that the dikes were emplaced perpendicular to the main shortening direction. The systematic locations of the dikes at the anticlinal hinges suggest that their emplacement was controlled by local, shallow stresses related to outer-arc stretching at the anticlinal hinge. We conclude that folding-related outer-arc stretching is one mechanism responsible for the vertical partitioning of igneous plumbing systems in compressional tectonic settings.

INTRODUCTION

There is growing evidence of close structural and temporal links between igneous plumbing systems and thrust faults (Fig. 1). Recent field observations (Foster et al., 2001; Kalakay et al., 2001; Musumeci et al., 2005; Ferré et al., 2012), seismic data (Araujo et al., 2013), and laboratory experiments (Galland et al., 2003; Musumeci et al., 2005; Galland et al., 2007a, 2008; Montanari et al., 2010; Ferré et al., 2012) suggest that magma can be transported along thrust faults. Active volcanoes such as Guagua Pichincha volcano (Ecuador; Legrand et al., 2002), El Reventador volcano (Ecuador; Tibaldi, 2005, 2008), Tromen volcano (Fig. 1A; Argentina; Marques and Cobbold, 2006; Galland et al., 2007b; Llambías et al., 2011), and several volcanoes in Atacama (northern Chile–Bolivia; Branquet and Van Wyk de Vries, 2001; González et al., 2009; Tibaldi et al., 2009; Acocella et al., 2011) are, however, almost never located along the nearby thrust faults, but instead they are positioned at the top of the hanging wall of thrust faults, away from the actual fault surface.

Recent geophysical (Legrand et al., 2002; Tibaldi, 2005) and geological studies (González et al., 2009) suggest that magma does not only follow thrust faults all the way through the crust, but instead that the volcanic plumbing systems in compressional environments are vertically partitioned into: (1) a deep level subject to regional compression, likely controlled by thrust faults, and (2) a shallow level subject to local extension, controlled by local extensional fractures (Fig. 1C). Consequently, deep magma conduits are expected to be dominantly subhorizontal, whereas shallow magma conduits are expected to be mainly subvertical. This structural partitioning is very similar to that documented at mud volcanoes formed in fold-and-thrust belts, where: (1) the source of mud is mostly horizontal in a specific sedimentary formation, (2) mud volcanoes crown the top of thrust ramp anticlines, and (3) shallow mud conduits are inferred to be vertical and located along the hinge of the anticlines (Fig. 1B; Deville et al., 2003; Morley et al., 2010; Roberts et al., 2011). These observations, both from igneous and mud volcanoes, lead to the following questions: What mechanism controls the partitioning of emplacement depth and geometry between deep to shallow levels? At what depth does such transition occur?

There are several hypotheses that could explain the occurrence of the vertical partitioning of subvolcanic conduit orientations in compressional tectonic settings: (1) Rheological layering of the country rock controls the transition from subhorizontal to vertical conduits (Watanabe et al., 1999; Kavanagh et al., 2006). (2) Local stresses due to folding (e.g., outer-arc stretching; Galland et al., 2009; Galland and Scheibert, 2013) or local tectonic structures cause magma pathways to deviate (Valentine and Krogh, 2006; Galland et al., 2007a; Bureau

†Current address: Department of Earth Sciences, University of Utrecht, P.O. Box 80021, 3508 TA Utrecht, The Netherlands; derya.guerer@gmail.com.

 doi: 10.1130/B31341.1; 13 figures; 1 table; Data Repository item 2015284.

Geological Society of America Bulletin, published online on 2 September 2015 as doi:10.1130/B31341.1

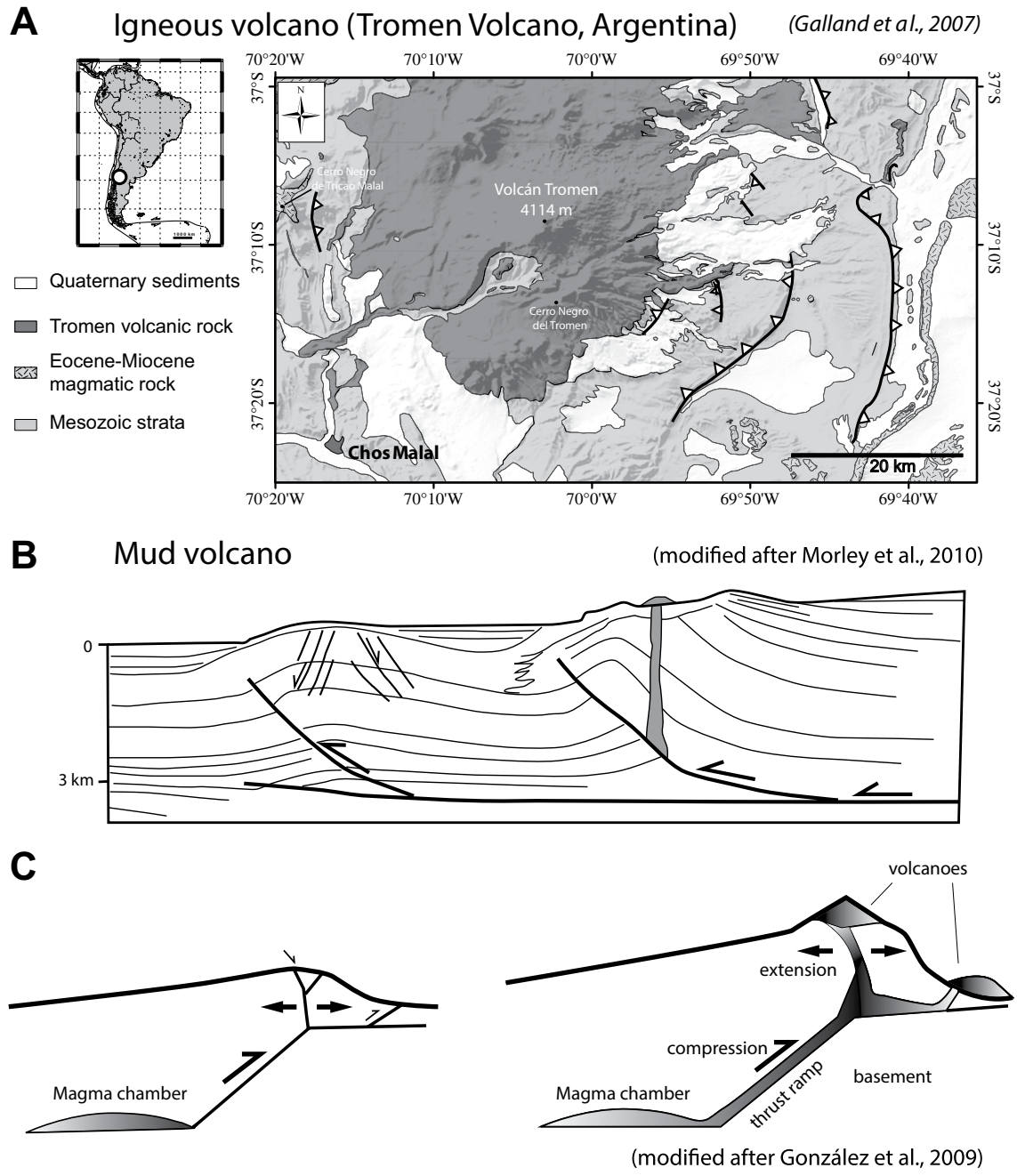

Figure 1. Characteristic examples of igneous and mud volcanoes formed in fold-and-thrust belts. (A) Structural map of Tromen volcano, Neuquén Province, Argentina, modified from Galland et al. (2007b). Tromen volcano crowns the thrust ramp anticline of an east-verging Tromen Thrust. (B) Schematic cross section of characteristic relationships between mud volcanoes (gray) and ramp anticlines in fold-and-thrust belts, modified from Morley et al. (2010). Mud volcanoes also crown thrust ramp anticlines. (C) Schematic drawing of a partitioned volcano plumbing system in fold-and-thrust belts, modified from González et al. (2009).

et al., 2013; Magee et al., 2013). (3) Local stresses due to the weight of a volcanic edifice control the formation of vertical magma conduits (e.g., Tibaldi, 2008; González et al., 2009; Kervyn et al., 2009; Tibaldi et al., 2014). These hypotheses have been proposed based only on either indirect observations (González et al., 2009), or pure tectonic models with no magma injection (Tibaldi, 2008). In addition, none of the existing models of magma emplacement in a shortening crust reproduces this partitioning of magma conduit orientation (Musumeci et al., 2005; Galland et al., 2007a; Montanari et al., 2010).

To test the relevance of this partitioning, to document it, and to constrain the mechanisms governing it, one needs direct geological observations of: (1) the structure of exhumed volcanic plumbing systems in fold-and-thrust belts, and (2) the relationships between these plumbing systems and associated tectonic

Geological Society of America Bulletin, published online on 2 September 2015 as doi:10.1130/B31341.1

structures. Hence, we document detailed structural and geochronological data from the Cerro Negro intrusive complex, which was emplaced in the Chos Malal fold-and-thrust belt in the foothills of the Neuquén Andes, in Argentina (Kozlowski et al., 1996; Cobbold and Rossello, 2003; Turienzo et al., 2014). The Cerro Negro intrusive complex is an ideal case study because its plumbing system and the adjacent tectonic structures of the Chos Malal fold-and-thrust belt are exhumed and well exposed (Zöllner and Amos, 1973).

GEOLOGICAL SETTING

The Cerro Negro de Tricao Malal (2520 m) is located in the western part of the Neuquén Basin, northern Neuquén Province, Argentina (Fig. 2). The Neuquén Basin is part of an extensional system, which was developed in a retro-arc context along the active margin of South America. It contains Late Triassic to early Paleogene marine and continental sequences, up to 6000 m in thickness, accumulated in a variety of conditions (Uliana and Legarreta, 1993; Legarreta and Uliana, 2001), which we describe next. The western margin of the basin is bounded by an almost continuous volcanic arc (Fig. 2).

The oldest Mesozoic rocks cropping out in the study area are the uppermost part (120 m thickness) of the Upper Jurassic–Lower Cretaceous organic-rich mudstone of the Vaca Muerta Formation, the Lower Cretaceous sandstone of the Mulichinco Formation (250 m thickness), and two sequences of organic-rich mudstones of the Agrio Formation (Weaver, 1931). The Lower Agrio shales, known as the Pilmatué Member (600 m thickness), and the Upper Agrio shales, termed the Agua de la Mula Member (Leanza et al., 2001), are separated by a conspicuous fluvio-eolian sandstone known as the Avilé Member (Fig. 3; Weaver, 1931). In the study area, the Avilé Member is 150–180 m thick (Veiga et al., 2002), and we estimated the thickness of the Agua de la Mula Member to 150 m based on mapping arguments. These formations were deposited in a postrifting subsidence setting (Howell et al., 2005). The Agua de la Mula Member is unconformably covered by fluvial sandstones and playa-lake muds of the Lower Troncoso Member (45 m thickness) and evaporitic deposits of the Upper Troncoso Member (15 m thickness) of the Huitrín Formation (Kozlowski et al., 1996; Guerello, 2006). The unconformity between the Agrio Formation and the Huitrín Formation marks the onset of compressional deformation and the beginning of sedimentation in a foreland setting (Cobbold and Rossello, 2003; Leanza, 2009; Tunik et al., 2010). Younger, mainly lacustrine reddish deposits of the Rayoso Formation and the red deposits of the Neuquén Group represent clastic deposition in a continental setting (Fig. 3). Pliocene–Pleistocene aggradational deposits also crop out in the core of a syncline between the Cerro Negro and the Cordillera del Viento (Fig. 2; Leanza, 2010).

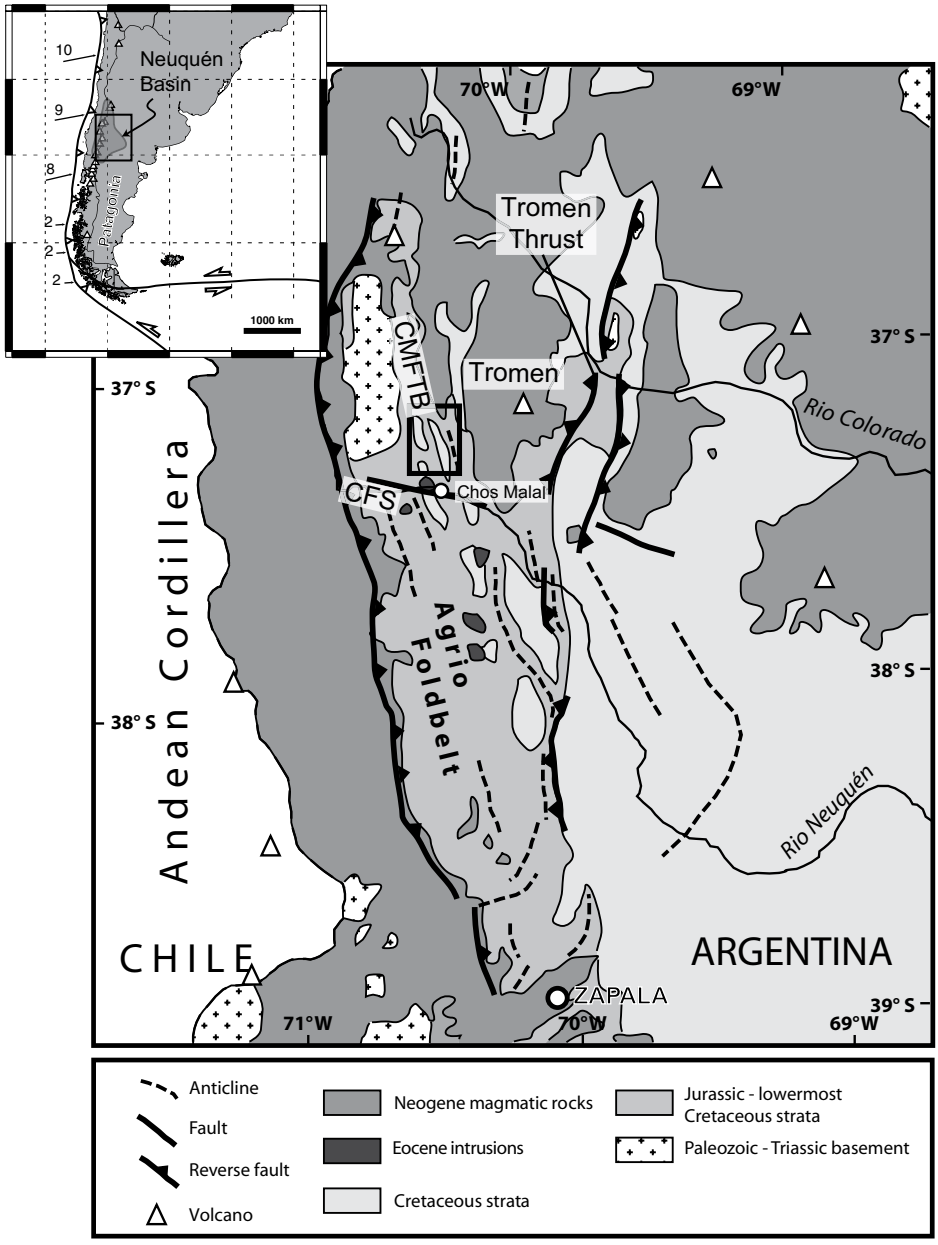

Figure 2. Simplified geological map of the Neuquén Basin, northwestern Neuquén Province, modified from Cobbold and Rossello (2003) and Galland et al. (2007b). Map shows main groups of sedimentary and magmatic rocks, major tectonic structures, and principal volcanoes (white triangles). CFS denotes the regional-scale Cortaderas fault system (e.g., Cobbold and Rossello, 2003). Box indicates area around Cerro Negro de Tricao Malal, north of Chos Malal, within the Chos Malal fold-and-thrust belt (CMFTB). Inset shows large-scale tectonic setting; numbers denote current velocity vectors for Nazca plate relative to South America (cm/yr).

The Cerro Negro intrusive complex is located north of the Cortaderas fault system (Fig. 2), a major regional lineament, to the north of which Eocene to Holocene back-arc magmatic rocks are widespread, and shortening is more pronounced than to the south (Kay et al., 2006; Ramos and Kay, 2006). The Cerro Negro intru-

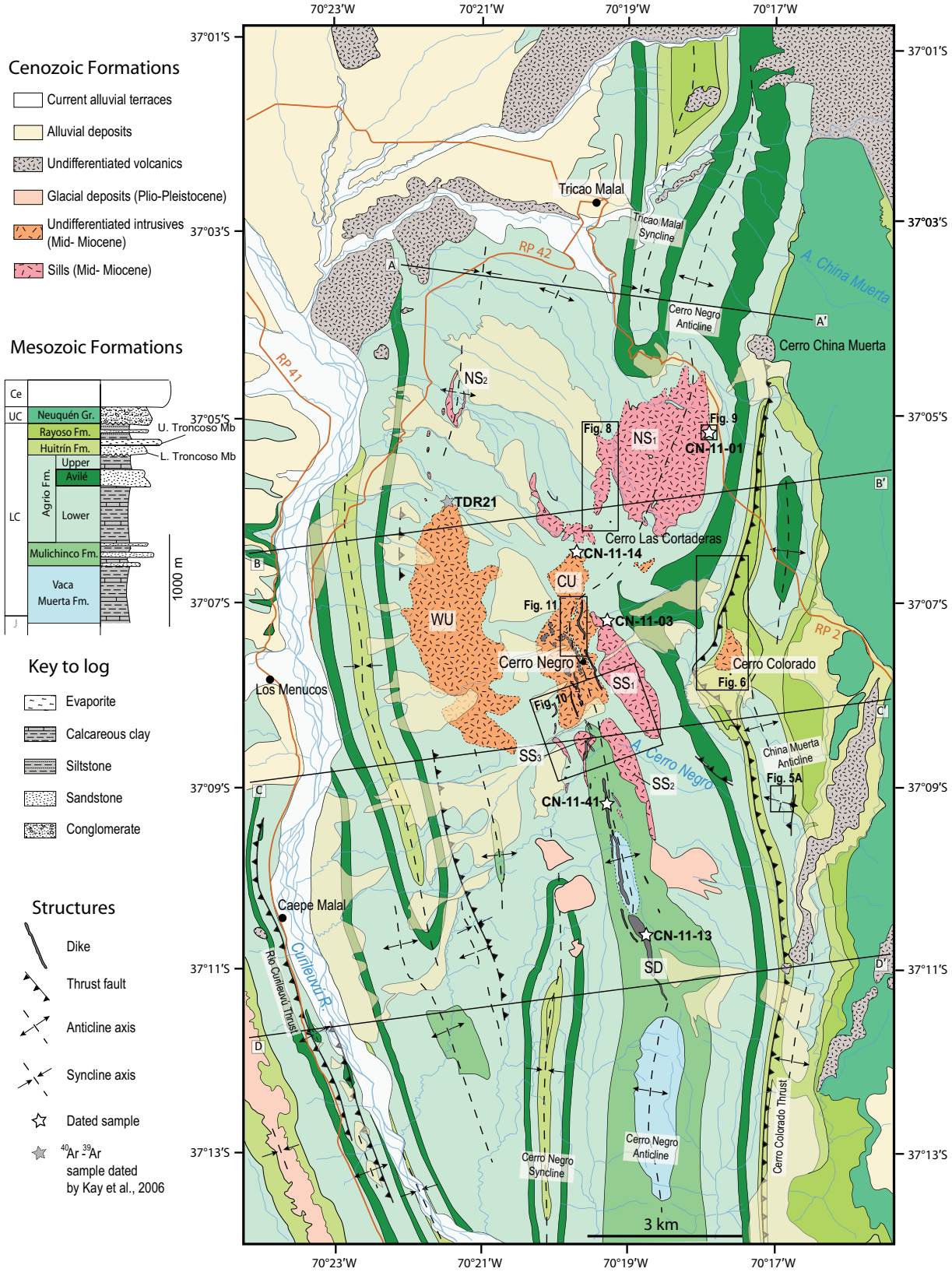

Figure 3. Geological map of the Cerro Negro intrusive complex and surrounding structures. The simplified stratigraphic column of the Neuquén Basin in the study area (left) is modified after Kozlowski et al. (1996) and Galland et al. (2007b). Black straight lines locate geological cross sections of Figure 4. CU—Central unit; WU—Western unit; SS_1—Southern Sill 1; SS_2—Southern Sill 2; SS_3—Southern Sill 3; NS_1—Northern Sill 1; and NS_2—Northern Sill 2; SD—Southern Dike. J—Jurassic; LC—Lower Cretaceous; UC—Upper Cretaceous; Ce—Cenozoic.

Geological Society of America Bulletin, published online on 2 September 2015 as doi:10.1130/B31341.1

sive complex was emplaced within the Chos Malal fold-and-thrust belt (Kozlowski et al., 1996; Sánchez et al., 2013; Turienzo et al., 2014), north of the Agrio fold belt (Fig. 2).

The Chos Malal fold-and-thrust belt is developed between the Cordillera del Viento (Paleozoic basement) to the west (Llambías et al., 2007) and the Tromen Massif, with its volcanic products, to the east (Galland et al., 2007b; Llambías et al., 2011). As a result of intense shortening, the Chos Malal fold-and-thrust belt exhibits a complex framework of thrust faults, associated with tight anticlines and synclines (Sánchez et al., 2013; Turienzo et al., 2014). It is the result of a long and complex tectonic evolution, with three main phases of shortening: the Patagonidican phase (Aptian to Campanian), the Incaican phase (Eocene), and the Quechua phase (Neogene; Groeber, 1929; Cobbold and Rossello, 2003). The Neogene tectonic evolution of the Chos Malal fold-and-thrust belt is debated. Kozlowski et al. (1996) and Folguera et al. (2007) argued that the main compressional phase ended before 12 Ma. Several authors claim that the area was subject to back-arc extension during the last 5 m.y. (Folguera et al., 2006b; Kay et al., 2006; Ramos and Kay, 2006; Folguera et al., 2008). Based on structural, geomorphic, and bore-hole evidence, Cobbold and Rossello (2003), Galland et al. (2007b), Folguera et al. (2007), Guzmán et al. (2007), and Messager et al. (2010, 2014) concluded that compressional deformation is still active. Such discrepancies highlight the need to constrain the timing of deformation to better understand the temporal relationships for the emplacement of the Cerro Negro intrusive complex in the context of adjacent tectonic structures. Thus, determining whether shortening occurred during magmatism, or not, is a key question of our study.

The study area also experienced a complex igneous evolution since the Cretaceous (Cobbold and Rossello, 2003; Kay et al., 2006; Galland et al., 2007b; Ramos, 2009). The region hosts igneous rocks formed in the Upper Cretaceous (Cerro Varvarcó and Cerro Nevazón; Kay et al., 2006), Eocene (Collipilli Province south of Chos Malal, Fig. 2; Llambías and Rapela, 1988; Kay et al., 2006), Lower Miocene (Huantraico Formation; Ramos and Barbieri, 1988; Kay and Copeland, 2006), Upper Miocene (Cerro Negro; Kay et al., 2006), and Holocene (Tromen volcano; Kay et al., 2006; Galland et al., 2007b). Kay et al. (2006) interpreted the back-arc position of this magmatism as a result of evolving dip angle of the subduction slab to the west.

The structure and age of the Cerro Negro intrusive complex are poorly constrained. Zöllner and Amos (1973) mapped the complex as a massive intrusion, connected to a vertical dike at the core of an anticline to the south. They also mapped lavas in the surroundings of the intrusion, suggesting that the current level of exposure of the Cerro Negro intrusive complex is shallow (1–2 km depth). Llambías and Rapela (1988) correlated the intrusive rocks of the Cerro Negro intrusive complex with the Eocene volcanic Collipilli Formation based on their petrography, together with the Cerro Mayal and Cerro Caycayen located west and south of Chos Malal, respectively. In contrast, Kay et al. (2006) suggested that the intrusive complex may be Miocene, based on a $^{40}Ar/^{39}Ar$ age (11.7 ± 0.2 Ma) on hornblende from the western flank of the complex (Fig. 3).

STRUCTURAL OBSERVATIONS

To constrain the geometry of the Cerro Negro intrusive complex, and its structural and temporal relationships with the deformation observed in the Chos Malal fold-and-thrust belt, we conducted detailed mapping of the complex and adjacent structures, as well as U-Pb dating of zircons from the magmatic complex. The detailed description of our observations is provided as electronic supplementary material (Table DR1[1]), together with a full list of field localities (waypoints [WP]) with global positioning system (GPS) positions (degrees, minutes, seconds) and measurement descriptions. Structural measurements were corrected for magnetic declination and are presented as dip direction/dip angle for planar elements (bedding, faults, foliations). The stereograms in the figures display bedding planes (black dashed lines), fault planes (black solid lines), and intrusion/host contact planes (gray solid lines).

Structure of Chos Malal Fold-and-Thrust Belt

The most prominent structures observed in the study area are N-S–trending folds and N-S–striking faults (Fig. 3). The easternmost structure is the NNE-SSW–trending China Muerta anticline (Fig. 4; Guerello, 2006), which can be followed for 14 km (Fig. 3). Slightly to the southeast of the area of Figure 5A, small-scale reverse faults measured on the eastern flank of the anticline are compatible with WNW-ESE shortening, i.e., subperpendicular to the local fold axis (Fig. 5B). In addition, at the hinge of the China Muerta anticline, we locally observed normal faults dissecting the Troncoso sandstone, striking parallel to the local fold axis (Fig. 5B). The striations indicate ESE-WNW extension, likely due to outer-arc stretching localized at the hinge of the anticline. Note that the China Muerta anticline extends to the south as the Curileuvú anticline, as defined by Sánchez et al. (2013).

The west-verging Cerro Colorado thrust bounds the China Muerta anticline to the west (Fig. 4) and can be followed along the eastern margin of the study area for ~25 km (Fig. 3). It is best seen on the western flank of Cerro Colorado, where it offsets, and locally repeats, the Troncoso sandstone of the Huitrín Formation (Fig. 6). The presence of the Huitrín evaporite along the Cerro Colorado thrust (Fig. 3) suggests that it acted as décollement layer.

The main tectonic structure passing through the summit of Cerro Negro is the Cerro Negro anticline, which is continuous across the study area (Figs. 3 and 4). It exhibits along-strike wavelength variations, from ~1.5 km north of Cerro Negro to ~4 km at the Cerro Negro summit area (Fig. 4). The Cerro Negro anticline continues to the south of the Curileuvú River as the Las Maquinas anticline, defined by Sánchez et al. (2013) and Turienzo et al. (2014).

North and south of Cerro Negro intrusive complex, the Cerro Negro anticline passes laterally into a tight syncline to the west (Fig. 4). In the north, it was named Tricao Malal syncline by Guerello (2006). This syncline is not exposed west of the Cerro Negro intrusive complex (Fig. 3), and it is uncertain whether it is the same structure as the Cerro Negro syncline exposed south of the Cerro Negro intrusive complex (Figs. 3 and 4).

Between the Curileuvú River and Tricao Malal, the Lower Agrio shales crop out over a large area (Fig. 3; cross-section A-A′ in Fig. 4). The shales are very soft, and no continuous structure is observable in the landscape. Nevertheless, satellite image analysis of the area and the observation of a folded sill (NS_2; Fig. 3; see also next section) indicate the presence of tight anticlines and synclines of short wavelengths (Fig. 4). The hinge lines of these folds vary from N-S to NNE-SSW (Fig. 3). Directly to the west of the Cerro Negro intrusive complex, the slope is covered by debris, and only igneous rocks crop out (Fig. 3), so that no tectonic structure is observable (Fig. 3; cross-section B-B′ of Fig. 4).

Between the Cerro Negro anticline and the Curileuvú River, the folds of the southwestern part of the study area are well exposed and exhibit some complexity with along-strike

[1]GSA Data Repository item 2015284, Contains additional information on sample petrography (text and figures), major element geochemistry (text, figure, Table DR1) and zircon morphology (text, figures), and a full list of field localities (Table DR2) with corresponding structural measurements, is available at http://www.geosociety.org/pubs/ft2015.htm or by request to editing@geosociety.org.

Geological Society of America Bulletin, published online on 2 September 2015 as doi:10.1130/B31341.1

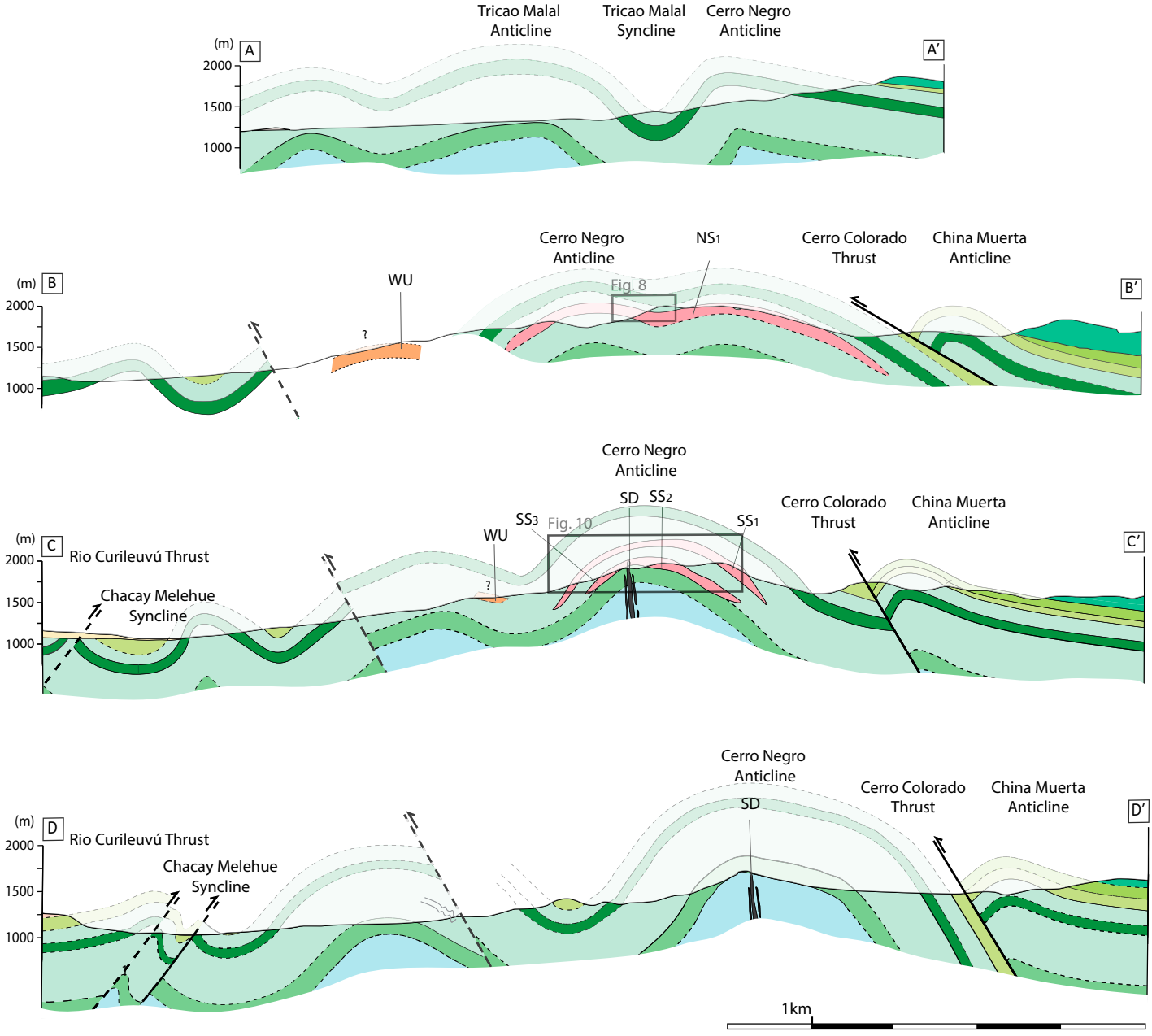

Figure 4. Geological cross sections across the Cerro Negro intrusive complex and surrounding areas (see locations in Fig. 3). Boxes locate geological observations of Figures 8 and 10. WU—Western unit; SD—Southern Dike. SS_1—Southern Sill 1; SS_2—Southern Sill 2; SS_3—Southern Sill 3; NS_1—Northern Sill 1; and NS_2—Northern Sill 2.

variations (Figs. 3, 4, and 7). Cross-section C-C′ (Fig. 4) shows the succession of anticlines and synclines, separated by a west-verging thrust. These structures do not continue southward (Figs. 3 and 4).

The Curileuvú thrust at the southwestern edge of the study area (Figs. 3 and 4) locally exhibits a duplex structure (Fig. 3; cross-section D-D′ of Fig. 4). The footwall of the Curileuvú thrust is characterized by a succession of tight folds, partly covered by the Curileuvú River (Fig. 3).

Structure of the Cerro Negro Intrusive Complex

In contrast to the depiction in the geological map of Zöllner and Amos (1973), the Cerro Negro intrusive complex does not correspond to a single massive intrusion, but it consists of several units.

The most prominent and spatially extensive units are sills. The main sill (northern sill 1, referred to as NS_1; Fig. 3) crops out over a large area because it is subparallel to the topography (cross-section B-B′, Fig. 4). We mainly observed its upper contact, but we locally also identified its lower contact (Fig. 8). It is dominantly concordant with the host rock stratigraphy (Lower Agrio shales), but local discordant contacts are common. It is folded into the Cerro Negro anticline, where the latter is 4 km wide (cross-section B-B′ of Fig. 4). The upper contact of NS_1 is well exposed in a small quarry to the east of the sill (Fig. 9).

Geological Society of America Bulletin, published online on 2 September 2015 as doi:10.1130/B31341.1

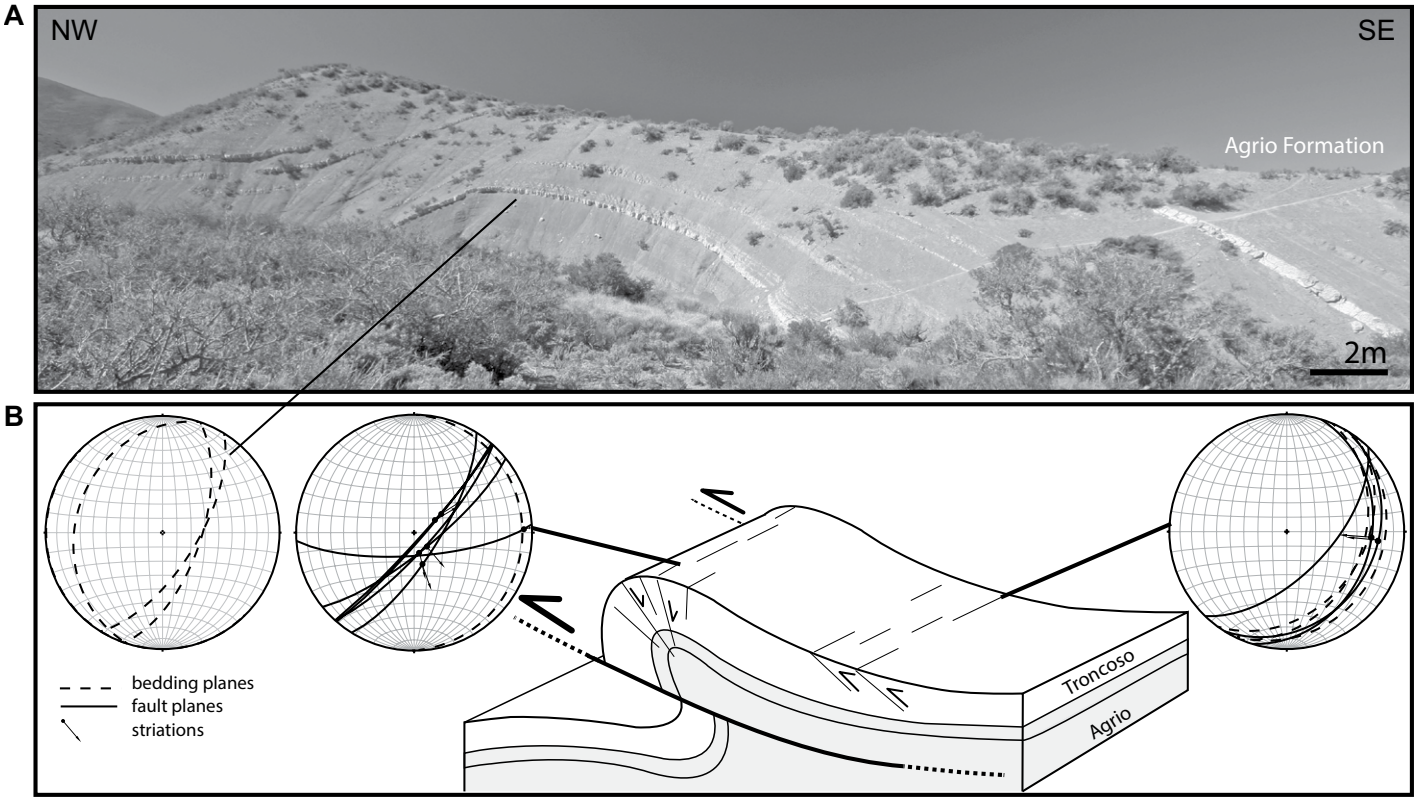

Figure 5. (A) Field photograph of the China Muerta anticline, looking N, south of Cerro Colorado (WP120–121; supplementary material [see text footnote 1]; location in Fig. 3). (B) Schematic diagram illustrating the location of fault plane measurements with respect to the China Muerta anticline. On its eastern flank (WP147; supplementary material [see text footnote 1]), reverse striated fault planes (solid lines) indicate E-W shortening. Fault planes are almost parallel to bedding (dashed lines). At the fold hinge (WP108; supplementary material [see text footnote 1]), normal faults strike parallel to the local axis of the China Muerta anticline and indicate ESE-WNW extension. The stereograms show strata measurements from the eastern and western limbs of the anticline, the intercept of which shows that the anticline axis trends NNW-SSE.

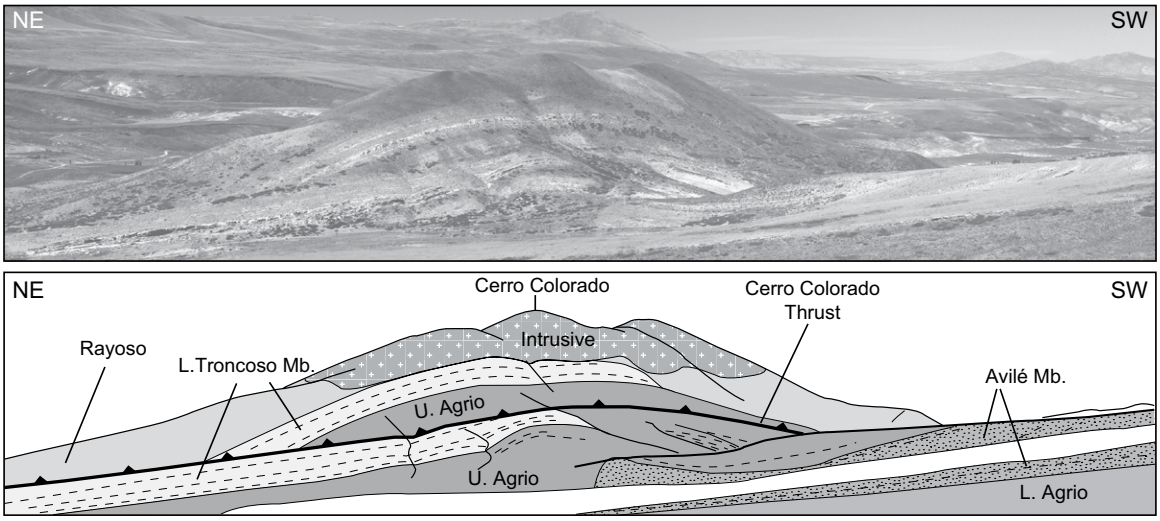

Figure 6. Field photograph of the western flank of Cerro Colorado (around 2 km in length; for location, see box in Fig. 3), view toward the ESE from WP47 (see supplementary material [see text footnote 1]). The west-verging Cerro Colorado thrust locally duplicates the Upper Troncoso sandstones. Dark lithology at the summit of Cerro Colorado is altered magmatic rock, which was mapped by Zöllner and Amos (1973) as the red sediments of the Rayoso Formation. Poor field exposure does not allow us to constrain the shape of the Cerro Colorado intrusion.

Geological Society of America Bulletin, published online on 2 September 2015 as doi:10.1130/B31341.1

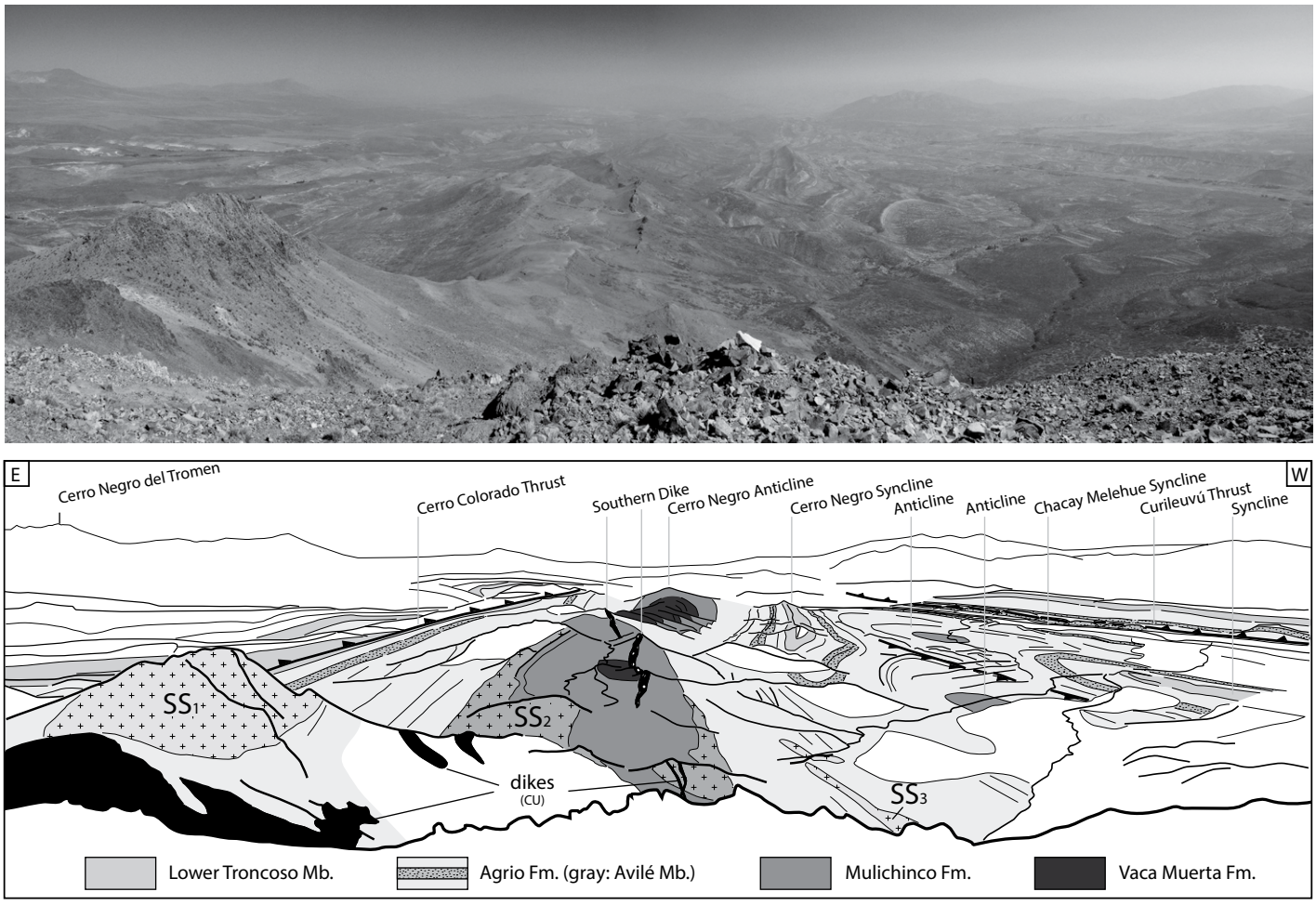

Figure 7. Overview of the southern part of the Cerro Negro intrusive complex and associated tectonic structures of the Chos Malal fold-and-thrust belt, looking S from the summit of Cerro Negro. The field of view is around 10 km in the central part of the image. CU—Central unit.

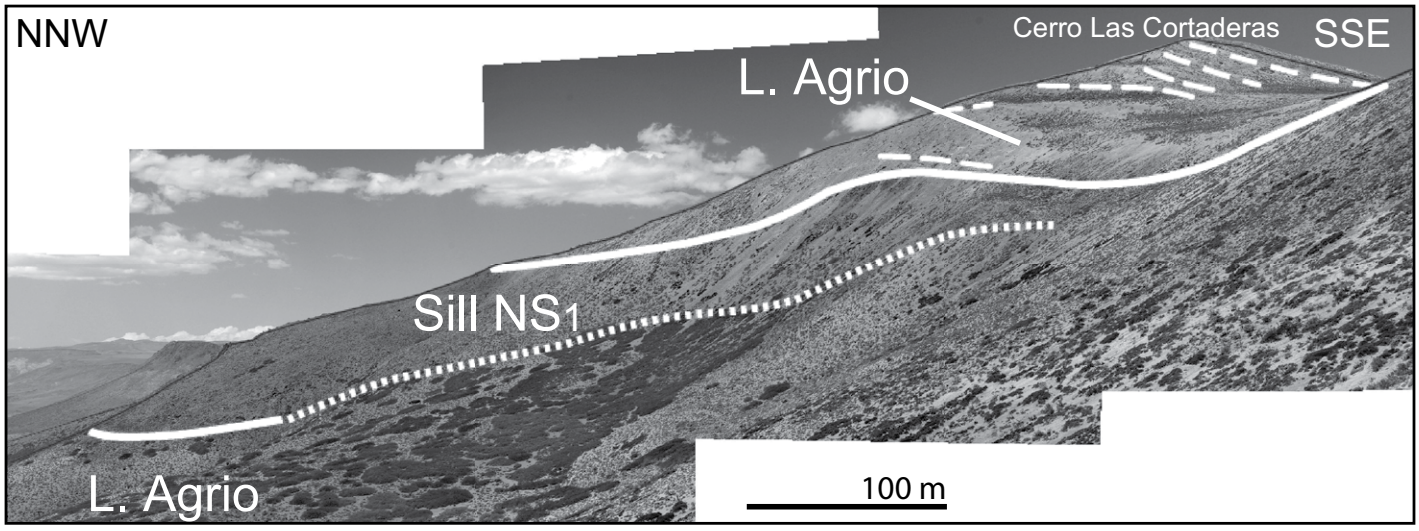

Figure 8. Interpreted field photograph of the northwestern part of northern sill 1 (NS_1; location in Fig. 3; cross-section B-B′ in Fig. 4). The lower contact of NS_1 crops out locally (lower-left corner; WP253; supplementary material [see text footnote 1]). The contacts (solid white line) are dominantly concordant with respect to the layering of the host Agrio shale (dashed white line).

Geological Society of America Bulletin, published online on 2 September 2015 as doi:10.1130/B31341.1

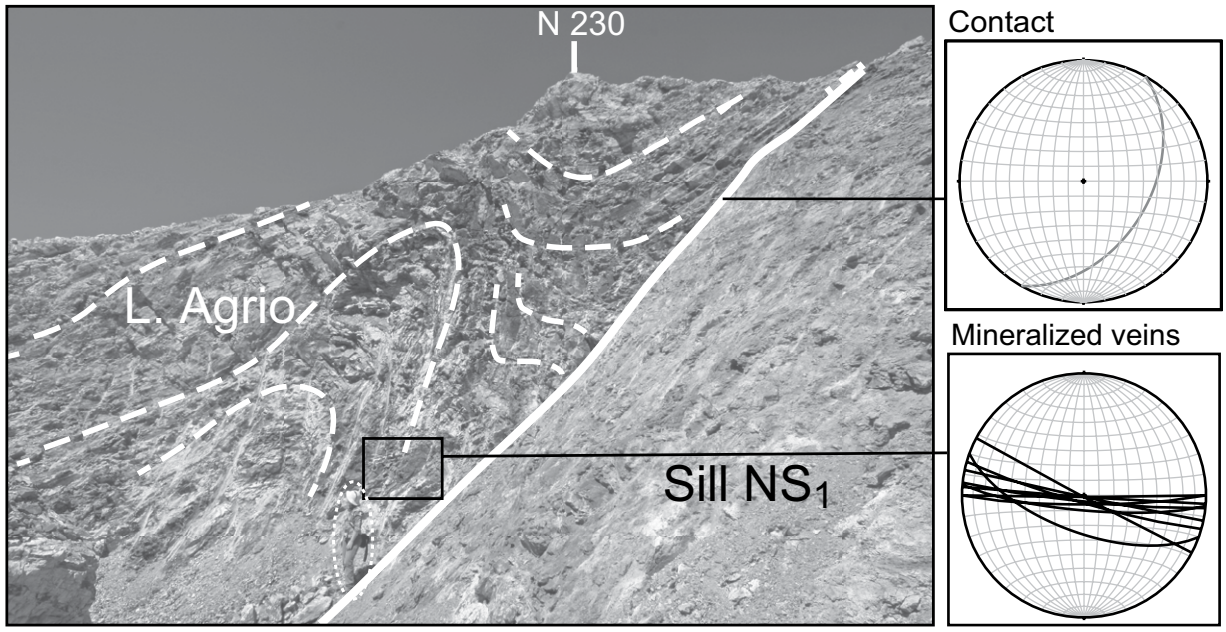

Figure 9. Interpreted field photograph of the upper contact of NS_1 exposed in a quarry, at the eastern side of NS_1 (WP18; supplementary material [see text footnote 1]; location in Fig. 3; cross-section B-B′ in Fig. 4). The Lower Agrio shales (dashed white lines) exhibit strong folding, where intense fracturing can be observed. Among the numerous fractures, E-W–striking ones are mineralized (lower-right stereogram). The contact is dipping to the east (upper-right stereogram). Away from the contact, the main bedding orientation is approximately subparallel to the contact. Small person for scale.

In this quarry, the Agrio shales are intensely dissected by joints, some of which are mineralized and dominantly strike E-W (Fig. 9).

A folded sill (northern sill 2, referred to as NS_2) is also exposed at the foot of the northwestern flank of Cerro Negro (Fig. 3) along both limbs of an anticline, so that its outcrop distribution exhibits an elliptical shape (Fig. 3). The rocks of NS_2 are strongly altered and light-brown-yellow to orange in color, and their magmatic fabric is hard to recognize.

Three main sills (SS_1, SS_2, and SS_3) are exposed at the southern flank of Cerro Negro (Figs. 3, 4, and 7). Sills SS_1 and SS_3 were emplaced in the middle, and sill SS_2 was emplaced at the bottom of the Lower Agrio shales (cross-section C-C′ of Fig. 4). Sill SS_1 forms a prominent ridge directly southeast of the summit of Cerro Negro (Figs. 7 and 10), along the eastern limb of the Cerro Negro anticline (cross-section C-C′ of Fig. 4). Both the upper and lower contacts are well exposed and associated with a layer of baked shale. The second thick sill (SS_2), consisting of altered yellowish andesite, is located south of the summit of Cerro Negro (Figs. 3, 7, and 10). The third sill (SS_3) crops out on the western limb of the Cerro Negro anticline (cross-section C-C′ in Fig. 4; Figs. 7 and 10). The similar andesitic mineralogy, chemical composition (supplementary material [see footnote 1]; Gürer, 2012), texture, and stratigraphic position of SS_1 and SS_3 suggest that they correspond to the same large sill exposed on both limbs of the Cerro Negro anticline (cross-section C-C′ of Fig. 4).

A prominent feature to the south of the Cerro Negro intrusive complex is a thick, 6-km-long dike of andesitic composition, which strikes roughly N-S (southern dike, referred to as SD; Figs. 3, 4, and 7; supplementary material [see footnote 1]). Locally, the southern dike exhibits several parallel dikes. Note that the southern dike crops out in the core, and is parallel to the axis, of the Cerro Negro anticline (cross-sections C-C′ and D-D′ in Fig. 4).

The central part of the Cerro Negro intrusive complex, named the Central unit (CU), is structurally the most complex. Near the summit of Cerro Negro, we observed a dense swarm of intrusions of variable compositions, separated by thin layers of baked limestone and shale of the Agrio Formation (Fig. 11). The contacts between the Agrio shales and intrusions (marked by chilled margins) are both concordant (subhorizontal) and discordant (vertical; stereogram in Fig. 11); many of these dikes strike N-S. They appear darker in the field than the sills and continuous in the landscape, suggesting that some of the dikes, at least, crosscut the sills. These dikes continue to the south, and some of them have been observed to crosscut SS_2 (WP217 and WP227; see supplementary material [footnote 1]; cross-section C-C′ in Fig. 4; Figs. 7 and 10).

The Central unit dikes exhibit the same orientations as the southern dike and are located in its northern continuation (Fig. 3). Nevertheless, we observed neither the northern tip of the southern dike nor the southern tips of these dikes; therefore, it is unclear whether they are connected or not. Petrographically, these dikes appear darker and more mafic than the southern dike. This suggests that they were not connected at the time of emplacement.

To the west of Cerro Negro, there are vast areas of igneous rocks, termed the Western unit (WU; Fig. 3). Although this part of the field area is widely covered by talus derived from the summit of Cerro Negro, several outcrops of Agrio shales between the central part of the Cerro Negro intrusive complex and the Western unit suggest that the latter is a separate unit. The contacts between igneous and sedimentary rocks are, however, hidden, and, consequently, the structure of this unit is not constrained (cross-section B-B′ of Fig. 4).

Finally, the summit area of Cerro Colorado, a hill east of the Cerro Negro (Fig. 3), consists of orange to dark-red rocks (Fig. 6). These were previously mapped by Zöllner and Amos (1973)

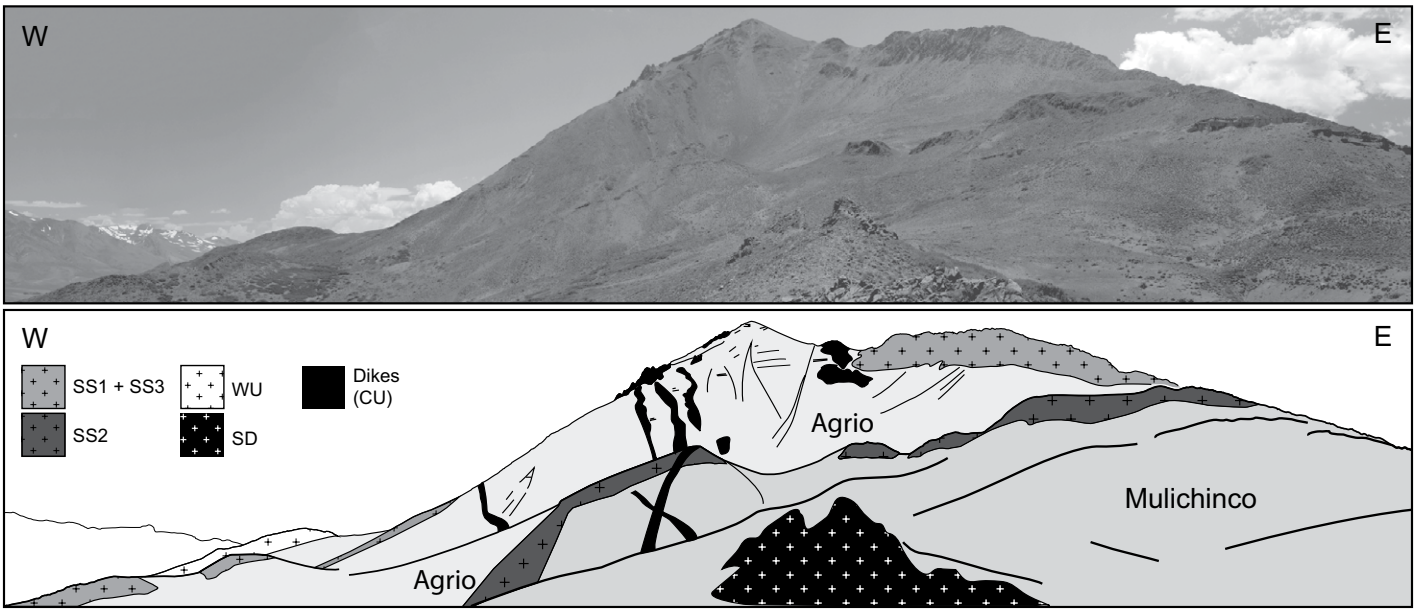

Figure 10. Field photograph (top) and corresponding interpretation (bottom) of the southern flank of Cerro Negro (field of view is ~2 km; see location in Fig. 3; cross-section C-C′ in Fig. 4), view toward the N from WP274 (supplementary material [see text footnote 1]). It displays the Southern Dike (SD) in the foreground, Southern Sill 1 (SS_1, crest to the right of main summit) and Southern Sill 2 (SS_2, intermediate ridge), Southern Sill 3 (SS_3, lower left), the Western unit (WU, behind SS_3), and the dikes of the Central unit (CU) crosscutting SS_2.

as being the sediments of the Rayoso Formation, but in fact they are very altered magmatic rocks. Due to poor outcropping conditions, no clear contacts between the intrusion and the surrounding Rayoso and Huitrín Formations were found (Fig. 6).

U-Pb AGES

Rationale for Sampling

Zircons in five samples were dated to verify whether the sills were coeval, or whether the N-E–striking dikes were systematically younger than the sills, and also to evaluate whether there was a chronological relationship between shortening in the Chos Malal fold-and-thrust belt and the dikes of the Cerro Negro intrusive complex.

The samples include two folded sills and three dikes. Sample CN-11-01 represents andesitic sill NS_1 (Fig. 9). At this locality, the sill is locally discordant, and mineralization has been observed at the contact. Sample CN-11-03 was collected from a sill on the eastern flank of Cerro Negro (SS_1, WP32; supplementary material [see footnote 1]), close to the contact with Agrio limestones. The three dikes include samples CN-11-13 and CN-11-41, from a dike south of Cerro Negro (WP185, WP274, respectively) and CN-11-14 from a small plug, which is part of a network of andesitic dikes north of the Cerro Negro summit (WP194).

Analytical Procedure

Dating was carried out by U-Pb isotope dilution–thermal ionization mass spectrometry (ID-TIMS), following a modified procedure of Krogh (1973) as detailed in Corfu (2004). Zircon grains were extracted by crushing, milling, and separation by means of a water table, magnetic separator, and heavy liquids. Zircon grains were selected under a binocular microscope and subjected to chemical abrasion (Mattinson, 2005, 2010) before spiking with a ^{202}Pb-^{205}Pb-^{235}U tracer, dissolution, and mass spectrometry. Because of the small amount of Pb available, measurement was done with an ion counting secondary electron multiplier. The obtained data were corrected with fractionation factors of 0.1%/amu for Pb and 0.12%/amu for U, subtracting blanks of 0.1 pg U and ≤2 pg Pb. The remaining initial Pb was corrected using compositions calculated with the model of Stacey and Kramers (1975). The data were also adjusted for a deficit of ^{206}Pb due to initial deficiency of ^{230}Th (Schärer, 1984). Plotting and regressions were done with the Isoplot software package (Ludwig, 2009). The decay constants are those of Jaffey et al. (1971). Uncertainties in the isotope ratios and the ages are given and plotted at 2σ (Table 1; Fig. 12).

Results

Zircon in all samples shows variations in morphology, ranging from long-prismatic to equant crystals, with sharp crystal faces and edges or more resorbed and subrounded morphologies. There are also variations in the intensity and size of inclusions, such as irregular melt channels and distinct minerals such as biotite, feldspar, and apatite. Analyses were carried out both on single- and multiple-grain fractions of zircon selected according to morphology and other characteristics.

The five samples yielded either coherent overlapping data sets or more scattered patterns. The latter reflect in part geological complexity, but, in some cases, likely also analytical complications due very small amounts of Pb available for analysis (Table 1; Fig. 12). An inherited component was found in sample CN-11-03, where four analyses yielded a discordia line with an upper-intercept age of ca. 1440 Ma, indicating a Mesoproterozoic age of the xenocrystic cores. The lower-intercept age of 11.58 ± 0.18 Ma indicates the time of magmatic crystallization and is identical within error to that of 11.63 ± 0.20 Ma provided by three overlapping analyses for the other dated sill CN-11-01. Zircons for two of the dikes, CN-11-13 and CN-11-14, yielded data that were scattered but roughly coincident with those of the sills, supporting an approximately coeval age of emplacement. More coherent results were obtained for sample CN-11-41, thanks also to the presence of larger zircon grains with better Pb levels for analysis. The five analyses yielded an average age of 11.55 ± 0.06 Ma, again identical within error to

Geological Society of America Bulletin, published online on 2 September 2015 as doi:10.1130/B31341.1

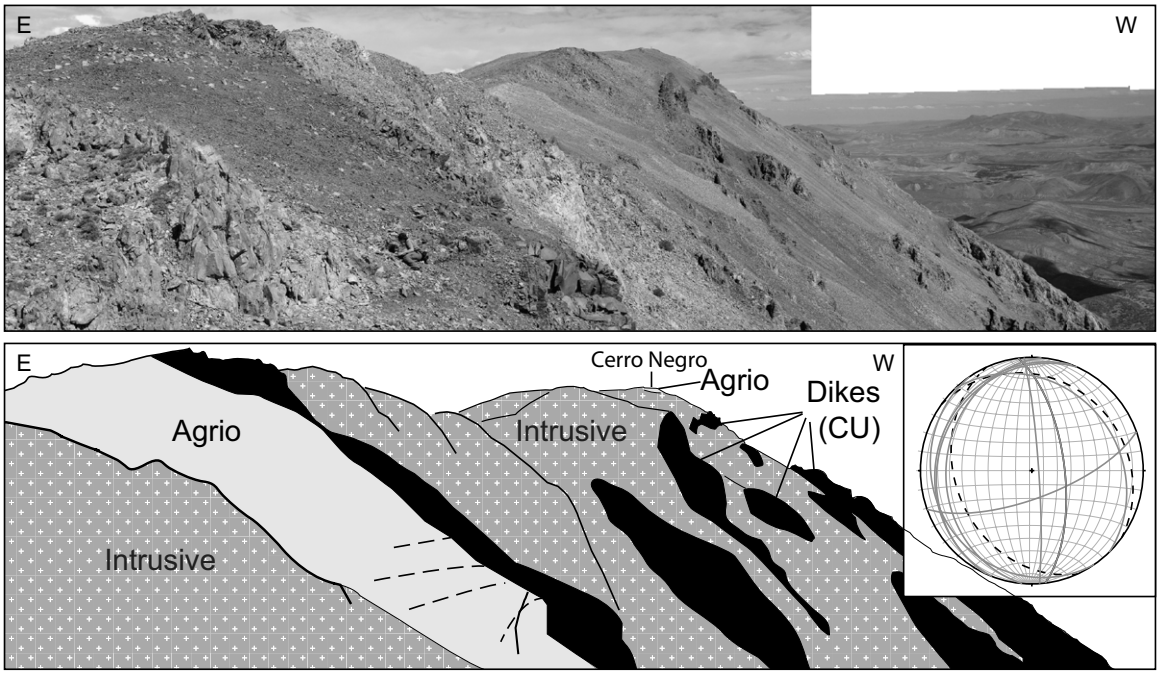

Figure 11. Field photograph (top) and corresponding interpretation (bottom) of the Central unit (CU) at the summit of Cerro Negro (field of view is ~1 km; see location in Fig. 3), looking toward the S from WP242 (supplementary material [see text footnote 1]). Despite access difficulties, it is possible to observe baked Agrio shales, and intrusions with both concordant and discordant contacts. The most prominent intrusions in the landscape are the dark N-S–striking dikes of the Central unit. The structure of the other, lighter, intrusions is hard to constrain, although measured concordant contacts (see stereogram) suggest that they are dominantly sills.

that of the two sills. In detail, one can observe a small internal variation from 11.64 Ma for an equant grain to 11.50 Ma for a long prism (Table 1) that may reflect progressive crystallization processes during magma evolution and emplacement, as is observed in other young magmatic systems (e.g., Schoene et al., 2012). However, the confirmation of the suggested sequence would require further work and a more extensive data set.

INTERPRETATION AND DISCUSSION

Timing of Sill and Dike Emplacement

Crosscutting relationships between dikes and sills have been observed at two localities (WP218 and WP227; supplementary material [see footnote 1]; Figs. 7 and 10) south of the Central unit, where dikes locally crosscut the folded sill (SS_2). Opposite relationships, i.e., sills crosscutting dikes, have not been observed. Furthermore, from the summit of Cerro Negro (Fig. 7), we observed that a swarm of N-S–striking dikes crosscuts all other units, sedimentary as well as magmatic. From these observations, we infer that the observed dikes are younger than the sills (Fig. 13).

The geochronological data obtained in this study indicate ages of 11.63 ± 0.20 Ma for NS_1, 11.58 ± 0.18 Ma for SS_1, and 11.553 ± 0.061 Ma for the southern dike. There are no resolvable age differences between the two distinct types of conduits, and the ages are similar to the $^{40}Ar/^{39}Ar$ age of 11.70 ± 0.20 Ma determined by Kay et al. (2006) for hornblende from the Western unit (sample TDR21 in Fig. 3). These ages suggest that magmatism in the study area was short-lived, with sill intrusion shortly predating dike intrusion.

One question concerns the geological meaning of the obtained ages: Do they correspond to the time of emplacement of the magma, the time of cooling of the bodies, or the time of formation of zircons as antecrysts in the magma chamber? The magmatic conduits observed at Cerro Negro intrusive complex are thin sheet intrusions. Their cooling time depends much on their depth of emplacement, i.e., the temperature of their host. Given that in the studied area the shale of the Agrio Formation experienced maximum maturation conditions in the oil window (Parnell and Carey, 1995; Legarreta et al., 2004), the maximum possible depth of emplacement of the Cerro Negro intrusive complex intrusions is ~4 km, and the intrusions likely solidified in a relatively short time. The zircons could have formed as antecrysts in the magma chamber, but the match between U-Pb zircon ages and the hornblende $^{40}Ar/^{39}Ar$ age indicates that any residence time of zircon in the magma chamber would have been short.

Age of Deformation versus Age of Magmatism

In the Neuquén Basin, compressional deformation started as early as the Late Cretaceous (e.g., Vergani et al., 1995; Cobbold and Rossello, 2003). In the Chos Malal fold-and-thrust belt, the main compressional deformation occurred during the Incaican (Paleogene) and the Quechua (Neogene) phases (e.g., Kozlowski et al., 1996; Cobbold et al., 1999; Cobbold and Rossello, 2003; Folguera et al., 2006a, 2007). The newly obtained Late Miocene U-Pb ages indicate that the Cerro Negro intrusive complex was emplaced during the Quechua phase, i.e., synchronous with shortening in the Chos Malal fold-and-thrust belt.

Regional geological correlations confirm that the area was experiencing contraction during the emplacement of the Cerro Negro intrusive complex. This is evidenced by the middle Mio-

Geological Society of America Bulletin, published online on 2 September 2015 as doi:10.1130/B31341.1

TABLE 1. ZIRCON U-Pb DATA, CERRO NEGRO INTRUSIVE COMPLEX

Properties*	Weight (ug)†	U (ppm)†	Th/U§	Pbc# (pg)	$^{206}Pb/^{204}Pb$**	$^{207}Pb/^{235}U$††	± 2s (abs)	$^{206}Pb/^{238}U$††	± 2s (abs)	rho	$^{207}Pb/^{206}Pb$††	± 2s (abs)	$^{206}Pb/^{238}U$†† (age in Ma)	± 2s	$^{207}Pb/^{235}U$†† (age in Ma)	± 2s
Sill (NS1) CN-11-01																
1 gr, br-pr	5	238	0.65	1.4	121	0.0126	0.0010	0.001876	0.000012	0.63	0.0486	0.0038	12.083	0.080	12.69	1.03
1 gr, res	3	76	0.49	1.1	42	0.0092	0.0040	0.001818	0.000032	0.66	0.037	0.016	11.71	0.20	9.26	4.01
1 gr, br-pr, res, in	1	392	0.00	1.1	58	0.0104	0.0027	0.001817	0.000023	0.83	0.041	0.010	11.70	0.15	10.48	2.72
1 gr, res	5	98	0.25	1.1	70	0.0098	0.0020	0.001797	0.000018	0.82	0.0394	0.0080	11.57	0.11	9.86	2.05
Sill (SS1) CN-11-03																
>10 gr, l-pr	36	98	0.42	17.0	50	0.0186	0.0016	0.002372	0.000027	0.12	0.0570	0.0050	15.27	0.17	18.74	1.63
10 gr, s-pr + eq	32	85	0.51	3.0	122	0.01180	0.00060	0.0018142	0.0000069	0.66	0.0472	0.0023	11.684	0.044	11.91	0.61
6 gr, l-pr, in	27	86	0.57	1.4	199	0.01133	0.00052	0.0017919	0.0000064	0.64	0.0459	0.0020	11.541	0.041	11.44	0.53
>10 gr, br-pr	45	86	0.67	1.0	435	0.01126	0.00022	0.0017814	0.0000045	0.50	0.0458	0.0008	11.474	0.029	11.37	0.22
Dike (CU) CN-11-14																
8 gr, s-pr, in	9	180	0.49	1.9	115	0.01135	0.00097	0.0018211	0.0000090	0.76	0.0452	0.0037	11.729	0.058	11.46	0.98
6 gr, l-pr, in	8	485	0.53	5.2	102	0.01149	0.00052	0.0017900	0.0000074	0.45	0.0466	0.0021	11.529	0.047	11.61	0.53
1 gr, l-pr, in	1	950	0.70	1.4	92	0.0103	0.0012	0.001766	0.000011	0.73	0.0423	0.0048	11.371	0.071	10.40	1.20
Dike (SD) CN-11-13																
5 gr, l-pr, in	10	96	0.90	2.9	55	0.0106	0.0018	0.001786	0.000017	0.70	0.0432	0.0070	11.50	0.11	10.75	1.79
1 gr, br-pr, pink	1	655	0.40	2.0	52	0.0085	0.0026	0.001685	0.000022	0.75	0.037	0.011	10.85	0.14	8.60	2.62
Dike (SD) CN-11-41																
1 gr,eq	26	49	0.44	2.1	87	0.0119	0.0013	0.001807	0.000013	0.70	0.0479	0.0049	11.636	0.081	12.03	1.27
1 gr, s-pr, oval	17	42	0.51	1.3	80	0.0116	0.0015	0.001801	0.000012	0.79	0.0469	0.0057	11.596	0.078	11.75	1.46
1 gr, br-pr, in	38	59	0.54	1.6	171	0.01173	0.00060	0.0017985	0.0000064	0.69	0.0473	0.0023	11.584	0.041	11.84	0.60
1 gr, s-pr	22	66	0.70	1.2	149	0.01173	0.00069	0.0017917	0.0000071	0.71	0.0475	0.0027	11.539	0.045	11.85	0.69
1 gr, l-pr	25	137	1.01	0.9	460	0.01134	0.00022	0.0017852	0.0000065	0.44	0.0461	0.0008	11.498	0.042	11.45	0.22

*Main features of analyzed zircon; l-pr—long prismatic (l/w = >4); s-pr—short prismatic; br-pr—broken prism; eq—equant; res—resorbed; in—inclusions: All zircon gains treated with chemical abrasion (Mattinson, 2005).

†Weight and concentrations are known to better than 10%, except those near the 1 ug limit of resolution of the balance.

§Th/U model ratio inferred from 208/206 ratio and age of sample.

#Total amount of common Pb (initial + blank).

**Raw data corrected for fractionation.

††Corrected for fractionation, spike, blank ($^{206}Pb/^{204}Pb$ = 18.3; $^{207}Pb/^{204}Pb$ = 15.555) and initial common Pb (based on Stacey and Kramers, 1975); error calculated by propagating the main sources of uncertainty.

The U-Pb ratio of the spike used in this work is adapted to $^{206}Pb/^{238}U$ = 0.015660 for the ET100 solution obtained with the ET2535 spike at the Natural Environment Research Council Isotope Geosciences Facilities.

The $^{206}Pb/^{238}U$ and $^{207}Pb/^{206}Pb$ values are corrected for excess ^{206}Pb assuming Th/U = 4 for the parent magma and using the equation of Schärer (1984).

cene synorogenic deposits of the Conglomerado Tralalhué Formation and Trapa Trapa Formation (described by Ramos, 1998; Repol et al., 2002; Leanza et al., 2006; Melnick et al., 2006), and the middle to late Miocene synorogenic deposits of the Pustos Burgos and Rincón Bayo Formations (Leanza et al., 2001; Zamora Valcarce et al., 2006; Folguera et al., 2011), observed in different parts of the Agrio fold-and-thrust belts. North of the Cerro Negro intrusive complex, in southern Mendoza, several synorogenic units show evidence of various phases of contraction, including one between ca. 11 and 8 Ma, i.e., during the emplacement of the Cerro Negro intrusive complex (Silvestro and Atencio, 2009).

The orientations of the mineralized veins observed in the small quarry on the eastern edge of NS_1 (Fig. 9) provide constraints on paleostress orientation. Although the host rock exhibits joints of various orientations, only the E-W–striking fractures are mineralized (lower-right stereogram in Fig. 9). This observation suggests that the maximum horizontal stress at the time of the formation of the mineralized veins was parallel (i.e., E-W) and the minimum horizontal stress was perpendicular (i.e., N-S) to the veins (e.g., Jolly and Sanderson, 1997; Bureau et al., 2013). This horizontal stress distribution is compatible with E-W compression. As the veins are concentrated in the vicinity of the sill–host-rock contact, we infer that their formation was coeval with the cooling of the sill, shortly after its emplacement. We therefore conclude that NS_1 was emplaced in a compressional stress regime (Fig. 13).

The main sills are dominantly concordant in a folded sequence (Figs. 4 and 10). Assuming that these sills were intruded as horizontal sheets, substantial shortening must have occurred during and/or after their emplacement at ca. 11.5 Ma.

The geological map (Fig. 3) and the geological cross sections (Fig. 4) show that (1) the folds and faults bend gently around the western flank of Cerro Negro, and (2) some folds exhibit along-strike variations in wavelength. These relationships between the along-strike variations of the tectonic structures and the location of the igneous units suggest that the igneous units have affected the structural development of the Chos Malal fold-and-thrust belt in the study area. This implies that substantial parts of the observed folding were developed after the emplacement of the Cerro Negro intrusive complex.

All these arguments are coherent with the emplacement of the Cerro Negro intrusive complex synchronous with the development of the Chos Malal fold-and-thrust belt (Fig. 13), unless the Quechua phase was discontinuous through time.

Geological Society of America Bulletin, published online on 2 September 2015 as doi:10.1130/B31341.1

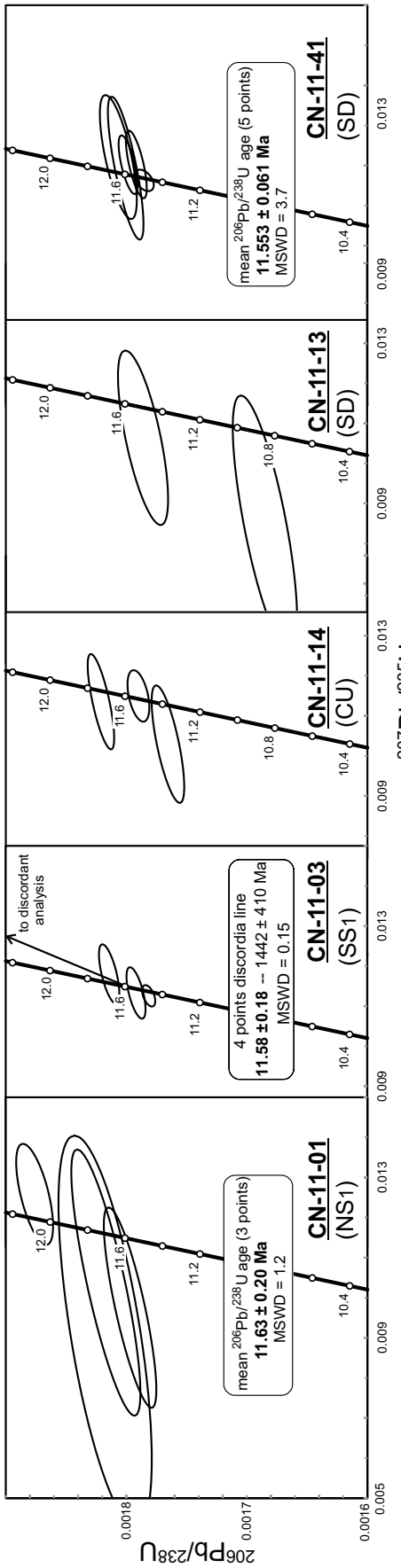

Figure 12. Concordia plots for zircons obtained from sills (CN-11-01, CN-11-03) and dikes (CN-11-13, CN-11-14, CN-11-41) of the Cerro Negro intrusive complex, with indication of the corresponding units. Ellipses indicate 2σ uncertainty. MSWD—mean square of weighted deviates. NS_1—northern sill 1; SS_1—southern sill 1; CU—Central unit; SD—southern dike.

Although we observed substantial shortening affecting the main sills, we did not observe deformation affecting the dikes of the Cerro Negro intrusive complex, possibly due to their location close to the hinge of the Cerro Negro anticline (Figs. 3, 4, 7, and 10). The dikes, however, have almost the same ages as the sills and, therefore, also have to be synkinematic (Fig. 13).

Mechanical Interpretation

The orientations of the dikes are perpendicular to the shortening direction, i.e., to the regional maximum principal stress σ_1, which is the exact opposite to theoretical predictions (Hubbert and Willis, 1957; Sibson, 2003). Nevertheless, we observed that all the N-S–striking dikes were emplaced close and parallel to the hinge of the Cerro Negro anticline (Figs. 3 and 4). Such systematic structural relationships between the dikes and the anticline cannot be a coincidence. It is known that folding produces complex local stress fields. In particular, local extension due to the fold's outer-arc stretching can occur in a regional compressional tectonic setting (Fig. 13). The normal faults locally observed at the hinge of the China Muerta anticline (Fig. 5), for example, are likely the result of outer-arc stretching, because (1) the small normal faults are parallel to the local fold axis, and (2) the extension appears perpendicular to the fold axis (Fig. 13). Although we did not observe structures associated with outer-arc stretching in the Cerro Negro anticline, it is likely that this mechanism is present there as well and controlled the emplacement of the observed N-S–striking dikes (Fig. 13). The peculiar orientations of these dikes with respect to the regional compressional tectonic stresses are thus likely due to local, shallow effects. This conclusion is in agreement with laboratory models, which produced local extensional fractures perpendicular to the regional compression at the hinge of thrust ramp anticlines (Galland et al., 2007a; Tibaldi, 2008).

In addition to outer-arc stretching, folding is also expected to produce inner-arc compression. In theory, these inner-arc stresses should have prevented the N-S–striking dikes observed in the Cerro Negro intrusive complex to intruding the inner part of the Cerro Negro anticline. The presence of the southern dike and dikes of the Central unit suggests other processes than pure tectonic folding. One possible explanation may be that thrusting at the core of the Cerro Negro anticline facilitated magma flow to the upper parts of the anticline. Another hypothesis is that the magmatic pressure at the core of the anticline was high enough to generate tensile

Geological Society of America Bulletin, published online on 2 September 2015 as doi:10.1130/B31341.1

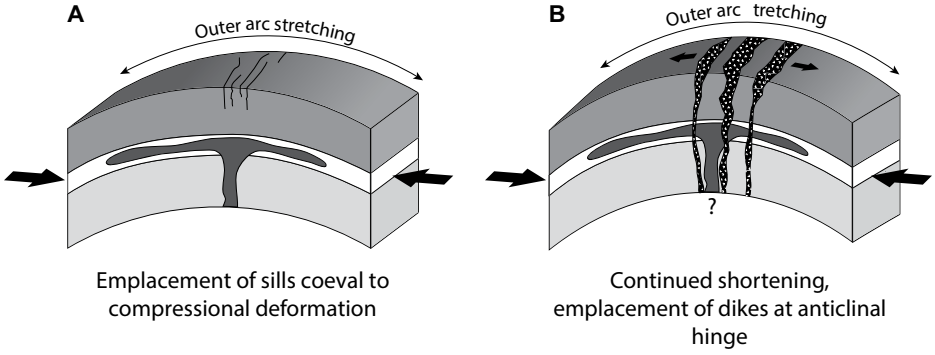

Figure 13. Schematic drawing of the two-stage magmatic evolution of the Cerro Negro intrusive complex with respect to the deformation history of the Chos Malal fold-and-thrust belt. Progressive folding leads to more pronounced outer-arc stretching, which becomes the dominant factor in controlling dike emplacement during stage B.

stresses even in the inner-arc zone of the anticline. Neither the root zone of the dikes nor the lower parts of the Cerro Negro anticline are exposed; therefore, these hypotheses cannot be tested.

There are striking differences between the structure of the igneous conduits observed in the Cerro Negro intrusive complex and that of the neighboring Tromen volcano (Galland et al., 2007b; Llambías et al., 2011); the vertical dikes observed at Tromen strike E-W, i.e., parallel to the shortening direction. Similar vertical dikes parallel to shortening have been observed, e.g., at Spanish Peaks, Colorado, USA, and have been interpreted as resulting from the interference between regional compressional stresses, where σ_1 and σ_3 are horizontal, interacting with an overpressurized vertical central conduit (Odé, 1957; Johnson, 1970; see also Nakamura, 1977). The model for Spanish Peaks, however, does not apply to Tromen, given that in the latter, (1) there is no evidence of a central vertical conduit, and (2) magmatism at Tromen was coeval with thrusting (Galland et al., 2007b; Llambías et al., 2011), i.e., regional σ_1 (E/W) and σ_2 (N/S) were horizontal, and σ_3 was vertical. Such a regional stress field is not compatible with the vertical E-W–striking dikes observed at Tromen volcano. We propose instead that the substantial weight of the 3-km-high Tromen edifice locally switched σ_2 to the vertical and σ_3 to the horizontal (N/S), controlling the E-W strikes of dikes. Such a process has been observed in the laboratory experiments of Galland et al. (2007a), which produced shortening-parallel open fractures when substantial topography was present. Furthermore, recently published experiments of Tibaldi et al. (2014) also documented the primordial influence of the load of a volcanic edifice on stress distributions and on dike patterns.

Conversely, the N-S–striking dikes at the Cerro Negro intrusive complex suggest that if a volcanic edifice was present at the time of their formation, it might have been relatively small, as its weight was not sufficient to control the emplacement of E-W–striking dikes.

The occurrence of both horizontal sills and vertical dikes at the hinge of anticlines of the Cerro Negro intrusive complex suggests distinct emplacement mechanisms (Fig. 13). This is in agreement with the model of vertical stress partitioning in volcanic plumbing systems in compression, in which "deep" levels are controlled by regional compression, and "shallow" levels are controlled by local effects (Fig. 1; Legrand et al., 2002; Tibaldi, 2008; González et al., 2009). The occurrence of both intrusion geometries in the study area suggests that the level of exposure was close to the transition zone between the "deep" and the "shallow" levels. Nevertheless, we did not observe a connection between the sills and the dikes (Fig. 13). Thus, our field observations do not allow us to estimate the depth of the transition between the deep and shallow levels.

The structure of the Cerro Negro intrusive complex is very similar to that of many mud volcanoes occurring in fold-and-thrust belts, such as in the Barbados accretionary prism (Deville et al., 2003), the Niger Delta and Brunei Darussalam (Morley et al., 2010), and Azerbaijan and Lusi mud volcano, Indonesia (Planke et al., 2003; Roberts et al., 2011). In these examples, the mud volcanoes erupt at the tips of thrust ramp anticlines, with the feeding conduits being vertical, parallel to the hinge of the anticlines. The sources of the mud are flat-lying overpressurized shale formations. The similarity between the Cerro Negro intrusive complex and these examples suggests that the formation of the vertical mud conduits is controlled by local stresses associated with outer-arc stretching. The similarities between igneous and mud volcano plumbing systems also suggest common underlying processes.

Implications for Regional Geology

The folded sills of the Cerro Negro intrusive complex recorded substantial shortening in the Chos Malal fold-and-thrust belt during the last 11 m.y. This confirms the conclusions of Cobbold and Rossello (2003), Galland et al. (2007b), Guzmán et al. (2007), Messager et al. (2010), and Sagripanti et al. (2015), among others, that compressional deformation prevailed during the Late Miocene. Conversely, this contradicts the conclusions of, e.g., Kozlowski et al. (1996) and Folguera et al. (2007), who suggested that the compressional deformation stopped before the emplacement of the Cerro Negro intrusive complex, based on the assumption that the igneous products of the latter were not deformed.

Our field observations do not allow us to constrain the age of the latest compressional deformation in the study area, as we did not observe geological units postdating deformation. The substantial amount of folding that affects the sills, however, suggests that compressional deformation prevailed at least until the Late Miocene. The recent compressional structures observed in the Andean foothills of the Neuquén Basin confirm this hypothesis (Cobbold and Rossello, 2003; Marques and Cobbold, 2006; Galland et al., 2007b; Messager et al., 2010, 2014). Our observations are not compatible with a shift to an extensional environment in the last 5 m.y., as suggested by, e.g., Kay et al. (2006), Ramos and Kay (2006), and Folguera et al. (2006b), because this would imply a fast and intense shortening episode between 11 and 5 Ma, directly followed by a regional extension, which seems unlikely.

Our U-Pb ages of 11.5–11.6 Ma for the Cerro Negro intrusive complex match the $^{40}Ar/^{39}Ar$ hornblende age of 11.7 Ma published by Kay et al. (2006). This confirms that the Cerro Negro intrusive complex is not related to the Eocene Collipilli volcanism (Llambías and Rapela, 1988), which includes the nearby Cerro Mayal and Cerro Caycayén intrusive complexes, despite their petrological similarities.

CONCLUSIONS

In this paper, we provide structural and geochronological data that document the structure and evolution of the Cerro Negro intrusive complex emplaced in the Chos Malal fold-and-thrust belt, northern Neuquén Province, Argentina. The main results of our study are:

(1) The Cerro Negro intrusive complex consists of sills emplaced in the Lower Agrio shales, and N-S–striking dikes. The dikes crosscut the sills.

(2) Zircon U-Pb ages of 11.63 ± 0.20 Ma and 11.58 ± 0.18 Ma for sills and 11.553 ± 0.061 Ma for a dike show that they were emplaced in a short period of time and confirm the $^{40}Ar/^{39}Ar$ age of Kay et al. (2006).

(3) Our ages and field observations demonstrate that the emplacement of the Cerro Negro intrusive complex was coeval with the tectonic development of the Chos Malal fold-and-thrust belt.

(4) The N-S–striking dikes were emplaced at the hinge of the Cerro Negro anticline, perpendicular to the shortening direction. We conclude that dike orientation was controlled by local, shallow stresses related to shallow outer-arc stretching at the anticlinal hinge zone.

(5) The latter formation of the dikes with respect to the sills suggests a progression in the growth of the Cerro Negro anticline during the evolution of the Cerro Negro intrusive complex.

(6) The folding affecting the sills shows that substantial shortening, leading to the current structure of the Chos Malal fold-and-thrust belt, prevailed during the last 11 m.y.

We conclude that folding-related outer-arc stretching is one mechanism responsible for the vertical partitioning of igneous plumbing systems in compressional tectonic settings.

ACKNOWLEDGMENTS

This study was supported by a Center of Excellence grant from the Norwegian Research Council to Physics of Geological Processes (PGP), Department of Geosciences, University of Oslo. A. Beinlich is specially thanked for assistance with field work preparations and practical matters regarding laboratory work in Oslo. G.B. Fjeld helped with mineral separation in the Oslo laboratory. R. Hoffbauer, University of Bonn, and U. Kasper and E. Hoffmann, University of Cologne, were helpful with acquiring geochemical data. P. Späthe, University of Würzburg, is thanked for excellent thin section preparation. We acknowledge valuable input from an earlier study, involving E. Rossello from Consejo Nacional de Investigaciones Científicas y Técnicas (CONICET) in Buenos Aires, and P.R. Cobbold from Géosciences Rennes, University of Rennes 1, France, funded by CONICET, Argentina. E.R. Neumann, University of Oslo, is thanked for help with petrographic work. D.J.J. van Hinsbergen is thanked for his valuable comments on an early version of the manuscript. We thank J. Bédard for editorial handling, as well as A. Folguera and A. Tibaldi for their constructive reviews.

REFERENCES CITED

Acocella, V., Gioncada, A., Omarini, R., Riller, U., Mazzuoli, R., and Vezzoli, L., 2011, Tectonomagmatic characteristics of the back-arc portion of the Calama–Olacapato–El Toro fault zone, Central Andes: Tectonics, v. 30, TC3005, doi:10.1029/2010TC002854.

Araujo, V.S., Dimieri, L.V., Frisicale, M.C., Turienzo, M.M., and Sánchez, N.P., 2013, Emplazamiento del cuerpo subvolcánico Laguna Amarga y su relación con las estructuras tectónicas andinas, sur de la provincia de Mendoza: Revista de la Asociación Geológica Argentina, v. 70, p. 40–52.

Branquet, Y., and Van Wyk de Vries, B., 2001, Effets de la charge des édifices volcaniques sur la propagation de structures régionales compressives: Exemples naturels et modèles expérimentaux: Comptes Rendus de l'Académie des Sciences. Ser. 2, Sciences de la Terre et des Planètes, v. 333, p. 455–461.

Bureau, D., Mourgues, R., Cartwright, J., Foschi, M., and Abdelmalak, M.M., 2013, Characterisation of interactions between a pre-existing polygonal fault system and sandstone intrusions and the determination of paleo-stresses in the Faroe-Shetland basin: Journal of Structural Geology, v. 46, p. 186–199, doi:10.1016/j.jsg.2012.09.003.

Cobbold, P.R., and Rossello, E.A., 2003, Aptian to Recent compressional deformation, foothills of Neuquén Basin, Argentina: Marine and Petroleum Geology, v. 20, p. 429–443, doi:10.1016/S0264-8172(03)00077-1.

Cobbold, P.R., Diraison, M., and Rossello, E.A., 1999, Bitumen veins and Eocene transpression, Neuquén Basin, Argentina: Tectonophysics, v. 314, p. 423–442, doi:10.1016/S0040-1951(99)00222-X.

Corfu, F., 2004, U-Pb age, setting and tectonic significance of the anorthosite-mangerite-charnockite-granite suite, Lofoten-Vesterålen, Norway: Journal of Petrology, v. 45, p. 1799–1819, doi:10.1093/petrology/egh034.

Deville, E., Mascle, A., Guerlais, S., Decalf, C., and Colletta, B., 2003, Lateral changes of frontal accretion and mud volcanism processes in the Barbados accretionary prism and some implications, *in* Bartolini, C., ed., Mexico and the Caribbean Region: Plate Tectonics, Basin Formation and Hydrocarbon Habitats: American Association of Petroleum Geologists Memoir 79, p. 1–19.

Ferré, E., Galland, O., Montanari, D., and Kalakay, T., 2012, Granite magma migration and emplacement along thrusts: International Journal of Earth Sciences, v. 101, p. 1–16, doi:10.1007/s00531-012-0747-6.

Folguera, A., Ramos, V.A., González Díaz, E.F., and Hermanns, R.L., 2006a, Miocene to Quaternary deformation of the Guañacos fold-and-thrust belt in the Neuquén Andes between 37°S and 37°30′S, *in* Kay, S.M., and Ramos, V., eds., Evolution of an Andean Margin: A Tectonic and Magmatic View from the Andes to the Neuquén Basin (35°–39°S Lat.): Geological Society of America Special Paper 407, p. 247–266.

Folguera, A., Zapata, T.R., and Ramos, V.A., 2006b, Late Cenozoic extension and the evolution of the Neuquén Andes, *in* Kay, S.M., and Ramos, V., eds., Evolution of an Andean Margin: A Tectonic and Magmatic View from the Andes to the Neuquén Basin (35°–39°S Lat.): Geological Society of America Special Paper 407, p. 267–285.

Folguera, A., Ramos, V.A., Zapata, T., and Spagnuolo, M.G., 2007, Andean evolution at the Guañacos and Chos Malal fold and thrust belts (36°30–37°S): Journal of Geodynamics, v. 44, p. 129–148, doi:10.1016/j.jog.2007.02.003.

Folguera, A., Bottesi, G., Zapata, T., and Ramos, V.A., 2008, Crustal collapse in the Andean backarc since 2 Ma: Tromen volcanic plateau, southern Central Andes (36°40′–37°30′S): Tectonophysics, v. 459, p. 140–160, doi:10.1016/j.tecto.2007.12.013.

Folguera, A., Rojas Vera, E., Spagnuolo, M., García Morabito, E., Zamora Valcarce, G., Bottesi, G., Zapata, T., and Ramos, V.A., 2011, Depósitos sinorogénicos y tafrogénicos neógenos a cuaternarios, *in* Leanza, H.A., Arregui, C., Carbone, O., Danieli, J.C., and Vallés, J.M., eds., Geologia y Recursos Naturales de la Provincia del Neuquén, XVIII Congreso Geologico Argentino, Relatorio: Neuquén, Argentina, Asociación Geológica Argentina, p. 287–294.

Foster, D.A., Schafer, C., Fanning, C.M., and Hyndman, D.W., 2001, Relationships between crustal partial melting, plutonism, orogeny, and exhumation: Idaho-Bitterroot batholith: Tectonophysics, v. 342, p. 313–350, doi:10.1016/S0040-1951(01)00169-X.

Galland, O., and Scheibert, J., 2013, Analytical model of surface uplift above axisymmetric flat-lying magma intrusions: Implications for sill emplacement and geodesy: Journal of Volcanology and Geothermal Research, v. 253, p. 114–130, doi:10.1016/j.jvolgeores.2012.12.006.

Galland, O., de Bremond d'Ars, J., Cobbold, P.R., and Hallot, E., 2003, Physical models of magmatic intrusion during thrusting: Terra Nova, v. 15, p. 405–409, doi:10.1046/j.1365-3121.2003.00512.x.

Galland, O., Cobbold, P.R., de Bremond d'Ars, J., and Hallot, E., 2007a, Rise and emplacement of magma during horizontal shortening of the brittle crust: Insights from experimental modeling: Journal of Geophysical Research, v. 112, p. B06402, doi:10.1029/2006JB004604.

Galland, O., Hallot, E., Cobbold, P.R., Ruffet, G., and de Bremond d'Ars, J., 2007b, Volcanism in a compressional Andean setting: A structural and geochronological study of Tromen volcano (Neuquén Province, Argentina): Tectonics, v. 26, TC4010, doi:10.1029/2006TC002011.

Galland, O., Cobbold, P.R., Hallot, E., and De Bremond d'Ars, J., 2008, Magma-controlled tectonics in compressional settings: Insights from geological examples and experimental modelling: Bolletino della Società Geologica Italiana, v. 127, p. 205–208.

Galland, O., Planke, S., Neumann, E.R., and Malthe-Sørenssen, A., 2009, Experimental modelling of shallow magma emplacement: Application to saucer-shaped intrusions: Earth and Planetary Science Letters, v. 277, p. 373–383, doi:10.1016/j.epsl.2008.11.003.

González, G., Cembrano, J., Aron, F., Veloso, E.E., and Shyu, J.B.H., 2009, Coeval compressional deformation and volcanism in the central Andes, case studies from northern Chile (23°S–24°S): Tectonics, v. 28, TC6003, doi:10.1029/2009TC002538.

Groeber, P., 1929, Líneas Fundamentales de la Geología del Neuquén, Sur de Mendoza y Regiones Adyacentes: Ministerio de Agricultura, Dirección General de Minas, Geología y Hidrología Publicación 58, 109 p.

Guerello, R.R., 2006, Geología del Sector Norte de la Fosa de Chos Malal, Provincia de Neuquén [Licenciatura]: Buenos Aires, Argentina, Universidad de Buenos Aires, 119 p.

Gürer, M.D., 2012, The Structure and Evolution of Magmatic Complexes in Fold-and-Thrust Belts: A Case Study of Cerro Negro, Neuquén Province, Argentina [M.Sc. Thesis]: Oslo, Norway, University of Oslo, 144 p.

Guzmán, C.G., Cristallini, E.O., and Bottesi, G.L., 2007, Contemporary stress orientations in the Andean retroarc between 34°S and 39°S from borehole breakout analysis: Tectonics, v. 26, TC3016, doi: 10.1029TC001958.

Howell, J.A., Schwartz, E., Spalletti, L.A., and Veiga, G.D., 2005, The Neuquén Basin: An overview, *in* Howell, J.A., Schwartz, E., Spalletti, L.A., and Veiga, G.D., eds., The Neuquén Basin, Argentina: A Case Study in Sequence Stratigraphy and Basin Dynamics: Geological Society of London Special Publication 252, p. 1–14.

Hubbert, M.K., and Willis, D.G., 1957, Mechanics of hydraulic fracturing, *in* Hubbert, M.K., ed., Structural Geology: New York, Hafner Publishing Company, p. 175–190.

Jaffey, A.H., Flynn, K.F., Glendenin, L.E., Bentley, W.C., and Essling, A.M., 1971, Precision measurement of half-lives and specific activities of ^{235}U and ^{238}U: Physical Review C: Nuclear Physics, v. 4, p. 1889–1906, doi:10.1103/PhysRevC.4.1889.

Johnson, A.M., 1970, Physical Processes in Geology: San Francisco, California, Freeman, Cooper & Company, 592 p.

Jolly, R.J.H., and Sanderson, D.J., 1997, A Mohr circle construction for the opening of a pre-existing fracture: Journal of Structural Geology, v. 19, p. 887–892, doi:10.1016/S0191-8141(97)00014-X.

Kalakay, T.J., John, B.E., and Lageson, D.R., 2001, Fault-controlled pluton emplacement in the Sevier fold-and-thrust belt of southern Montana: Journal of Structural Geology, v. 23, p. 1151–1165, doi:10.1016/S0191-8141(00)00182-6.

Kavanagh, J.L., Menand, T., and Sparks, R.S.J., 2006, An experimental investigation of sill formation and propagation in layered elastic media: Earth and Planetary Science Letters, v. 245, p. 799–813, doi:10.1016/j.epsl.2006.03.025.

Kay, S.M., and Copeland, P., 2006, Early to middle Miocene backarc magmas of the Neuquén Basin: Geochemical consequences of slab shallowing and the westward drift of South America, *in* Kay, S.M., and Ramos, V., eds., Evolution of an Andean Margin: A Tectonic and Magmatic View from the Andes to the Neuquén Basin (35°–39°S Lat.): Geological Society of America Special Paper 407, p. 185–213.

Kay, S.M., Burns, W.M., Copeland, P., and Mancilla, O., 2006, Upper Cretaceous to Holocene magmatism and evidence for transient Miocene shallowing of the Andean subduction zone under the northern Neuquén Basin, *in* Kay, S.M., and Ramos, V., eds., Evolution of an Andean Margin: A Tectonic and Magmatic View from the Andes to the Neuquén Basin (35°–39°S Lat.): Geological Society of America Special Paper 407, p. 19–60.

Kervyn, M., Ernst, G.G.J., van Wyk de Vries, B., Mathieu, L., and Jacobs, P., 2009, Volcano load control on dyke propagation and vent distribution: Insights from analogue modeling: Journal of Geophysical Research, v. 114, B03401, doi:10.1029/2008JB005653.

Kozlowski, E.E., Cruz, C.E., and Sylwan, C.A., 1996, Geología estructural de la zona de Chos Malal, Cuenca Neuquina, Argentina, *in* Buenos Aires, Proceedings XIII Congreso Geológico Argentino y III Congreso de Exploración de Hidrocarburos, v. 1, p. 15–26.

Krogh, T.E., 1973, A low-contamination method for hydrothermal decomposition of zircon and extraction of U and Pb for isotopic age determinations: Geochimica et Cosmochimica Acta, v. 37, p. 485–494, doi:10.1016/0016-7037(73)90213-5.

Leanza, H.A., 2009, Las principales discordancias de Mesozoico de la Cuenca Neuqina según observaciones de superficie: Revista del Museo Argentino de Ciencias Naturales, v. 11, p. 145–184.

Leanza, H.A., 2010, Hoja Geológica 3769-III, Chos Malal, Provincias del Neuquén y Mendoza: Buenos Aires, Instituto de Geología y Recursos Minerales–El Servicio Geológico Minero Argentino, scale 1:250 000.

Leanza, H.A., Hugo, C.A., and Repol, D., 2001, Hoja Geológica 3969-I, Zapala, Provincia del Neuquén: Instituto de Geología y Recursos Minerales–El Servicio Geológico Minero Argentino Boletín 275, scale 1:250,000.

Leanza, H.A., Repol, D., Sruoga, P., Hugo, C.A., Fauqué, L.A., and Zanettini, J.C.M., 2006, Hoja Geológica 3769-31, Chorriaca (escala 1:250,000), Provincia del Neuquén: Instituto de Geología y Recursos Minerales–El Servicio Geológico Minero Argentino (Instituto de Estudios de Poblacion y Desarrollo [Dominican Republic]), Boletin 354, p. 1–93.

Legarreta, L., and Uliana, M.A., 2001, Jurassic–Cretaceous marine oscillations and geometry of backarc basin fill, central Argentine Andes, *in* Macdonald, D.I.M., ed., Sedimentation, Tectonics and Eustasy: Sea Level Changes at Active Margins: International Association of Sedimentologists Special Publication 12, p. 429–450.

Legarreta, L., Cruz, C.E., Vergani, G., Laffitte, G.A., and Villar, H.J., 2004, Petroleum mass-balance of the Neuquén Basin, Argentina: A comparative assessment of the productive districts and non-productive trends, *in* American Association of Petroleum Geologists International Conference and Exhibition Extended Abstracts: Cancun, Mexico, American Association of Petroleum Geologists, v. 88, p. 13.

Legrand, D., Calahorrano, A., Guillier, B., Rivera, L., Ruiz, M., Villagomez, D., and Yepes, H., 2002, Stress tensor analysis of the 1998–1999 tectonic swarm of northern Quito related to the volcanic swarm of Guagua Pichincha volcano, Ecuador: Tectonophysics, v. 344, p. 15–36, doi:10.1016/S0040-1951(01)00273-6.

Llambías, E.J., and Rapela, C.W., 1988, Las volcanitas de Collipilli, Neuquén (37°S) y su relación con otras unidades paleógenas de la cordillera: Revista de la Asociación Geológica Argentina, v. 44, p. 224–236.

Llambías, E.J., Leanza, H.A., and Carbone, O., 2007, Evolución tectono-magmática durante el Pérmico al Jurásico temprano en la Cordillera del Viento (37°05′S–37°15′S): Nuevas evidencias geológicas y geoquímicas del inicio de la cuenca Neuquina: Revista de la Asociación Geológica Argentina, v. 62, p. 217–235.

Llambías, E.J., Leanza, H.A., and Galland, O., 2011, Agrupamiento volcánico Tromen-Tilhue, *in* Leanza, H.A., Arregui, C., Carbone, O., Danieli, J.C., and Vallés, J.M., eds., Geologia y Recursos Naturales de la Provincia del Neuquén, XVIII Congreso Geologico Argentino, Relatorio: Neuquén, Argentina, Asociación Geológica Argentina, p. 627–636.

Ludwig, K.R., 2009, Isoplot 4.1. A Geochronological Toolkit for Microsoft Excel, Berkeley Geochronology Center Special Publication 4, 70 p.

Magee, C., Jackson, C.A.-L., and Schofield, N., 2013, The influence of normal fault geometry on igneous sill emplacement and morphology: Geology, v. 41, p. 407–410, doi:10.1130/G33824.1.

Marques, F.O., and Cobbold, P.R., 2006, Effects of topography on the curvature of fold-and-thrust belts during shortening of a 2-layer model of continental lithosphere: Tectonophysics, v. 415, p. 65–80, doi:10.1016/j.tecto.2005.12.001.

Mattinson, J.M., 2005, Zircon U-Pb chemical abrasion ("CA-TIMS") method: Combined annealing and multi-step partial dissolution analysis for improved precision and accuracy of zircon ages: Chemical Geology, v. 220, p. 47–66, doi:10.1016/j.chemgeo.2005.03.011.

Mattinson, J.M., 2010, Analysis of the relative decay constants of ^{235}U and ^{238}U by multi-step CA-TIMS measurements of closed-system natural zircon samples: Chemical Geology, v. 275, p. 186–198, doi:10.1016/j.chemgeo.2010.05.007.

Melnick, D., Rosenau, M., Folguera, A., and Echtler, H., 2006, Neogene tectonic evolution of the Neuquén Andes western flank (37°–39°S), *in* Kay, S.M., and Ramos, V., eds., Evolution of an Andean Margin: A Tectonic and Magmatic View from the Andes to the Neuquén Basin (35°–39°S Lat.): Geological Society of America Special Paper 407, p. 73–95.

Messager, G., Nivière, B., Martinod, J., Lacan, P., and Xavier, J.P., 2010, Geomorphic evidence for Plio–Quaternary compression in the Andean Foothills of the southern Neuquén Basin, Argentina: Tectonics, v. 29, TC4003, doi:10.1029/2009TC002609.

Messager, G., Nivière, B., Lacan, P., Hervouët, Y., and Xavier, J.-P., 2014, Plio–Quaternary thin-skinned tectonics along the crustal front flexure of the southern Central Andes: A record of the regional stress regime or of local tectonic-driven gravitational processes?: International Journal of Earth Sciences, v. 103, p. 929–951, doi:10.1007/s00531-013-0983-4.

Montanari, D., Corti, G., Sani, F., Ventisette, C.D., Bonini, M., and Moratti, G., 2010, Experimental investigation on granite emplacement during shortening: Tectonophysics, v. 484, p. 147–155, doi:10.1016/j.tecto.2009.09.010.

Morley, C.K., King, R., Hillis, R., Tingay, M., and Backé, G., 2010, Deepwater fold and thrust belt classification, tectonics, structure and hydrocarbon prospectivity: A review: Earth-Science Reviews, v. 104, p. 41–91, doi:10.1016/j.earscirev.2010.09.010.

Musumeci, G., Mazzarini, F., Corti, G., Barsella, M., and Montanari, D., 2005, Magma emplacement in a thrust ramp anticline: The Gavorrano Granite (Northern Apennines, Italy): Tectonics, v. 24, TC6009, doi:10.1029/2005TC001801.

Nakamura, K., 1977, Volcanoes as possible indicators of tectonic stress orientation—Principle and proposal: Journal of Volcanology and Geothermal Research, v. 2, p. 1–16, doi:10.1016/0377-0273(77)90012-9.

Odé, H., 1957, Mechanical analysis of the dike pattern of the Spanish Peaks area, Colorado: Geological Society of America Bulletin, v. 68, p. 567–576, doi:10.1130/0016-7606(1957)68[567:MAOTDP]2.0.CO;2.

Parnell, J., and Carey, P.F., 1995, Emplacement of bitumen (asphaltite) veins in the Neuquén Basin, Argentina: American Association of Petroleum Geologists Bulletin, v. 79, p. 1798–1815.

Planke, S., Svensen, H., Hovland, M., Banks, D.A., and Jamtveit, B., 2003, Mud and fluid migration in active mud volcanoes in Azerbaijan: Geo-Marine Letters, v. 23, p. 258–268, doi:10.1007/s00367-003-0152-z.

Ramos, V.A., 1998, Estructura del sector occidental de la faja plegada y corrida del Agrio, cuenca Neuquina, Argentina, *in* Proceedings of the 10th Congreso Latinoamericano de Geología: Buenos Aires, Argentina, p. 105–110.

Ramos, V.A., 2009, Anatomy and global context of the Andes: Main geologic features and the Andean orogenic cycle, *in* Kay, S.M., Ramos, V.A., and Dickinson, W.R., eds., Backbone of the Americas: Shallow Subduction, Plateau Uplift, and Ridge and Terrane Collision: Geological Society of America Memoir 204, p. 31–65.

Ramos, V.A., and Barbieri, M., 1988, El volcanismo cenozoico de Huantraico: Edad y relaciones isotopicas iniciales, provincia del Neuquen: Revista de la Asociacion Geologica Argentina, v. 43, p. 210–223.

Ramos, V.A., and Kay, S.M., 2006, Overview of the tectonic evolution of the southern Central Andes of Mendoza and Neuquén (35°–39°S latitude), *in* Kay, S.M., and Ramos, V.A., eds., Evolution of an Andean Margin: A Tectonic and Magmatic View from the Andes to the Neuquén Basin (35°–39°S Lat.): Geological Society of America Special Paper 407, p. 1–17.

Repol, D., Leanza, H.A., Sruoga, P., and Hugo, C.A., 2002, Evolución tectónica del Cenozoico de la comarca de Chorriaca, Provincia del Neuquén, Argentina, *in* Proceedings of the 15th Congreso Geológico Argentino: El Calafate, v. 3, p. 200–204.

Roberts, K.S., Davies, R.J., Stewart, S.A., and Tingay, M., 2011, Structural controls on mud volcano vent distributions: Examples from Azerbaijan and Lusi, east Java: Journal of the Geological Society of London, v. 168, p. 1013–1030, doi:10.1144/0016-76492010-158.

Sagripanti, L., Rojas Vera, E.A., Gianni, G.M., Folguera, A., Harvey, J.E., Farías, M., and Ramos, V.A., 2015, Neotectonic reactivation of the western section of the Malargüe fold and thrust belt (Tromen volcanic plateau, southern Central Andes): Geomorphology, v. 232, p. 164–181, doi:10.1016/j.geomorph.2014.12.022.

Sánchez, N.P., Turienzo, M.M., Dimieri, L.V., Araujo, V.S., and Lebinson, F., 2013, Evolución de las estructuras andinas en la faja corrida y plegada de Chos Malal: Interacción entre el basamento y la cubierta sedimentaria de la Cuenca Neuquina: Revista de la Asociación Geológica Argentina, v. 71, p. 233–246.

Schärer, U., 1984, The effect of initial ^{230}Th disequilibrium on young U-Pb ages: The Makalu case, Himalaya: Earth and Planetary Science Letters, v. 67, no. 2, p. 191–204, doi:10.1016/0012-821X(84)90114-6.

Schoene, B., Schaltegger, U., Brack, P., Latkoczy, C., Stracke, A., and Günther, D., 2012, Rates of magma differentiation and emplacement in a ballooning pluton recorded by U-Pb TIMS-TEA, Adamello batholith, Italy: Earth and Planetary Science Letters, v. 355–356, p. 162–173, doi:10.1016/j.epsl.2012.08.019.

Sibson, R.H., 2003, Brittle-failure controls on maximum sustainable overpressure in different tectonic regimes: American Association of Petroleum Geologists Bulletin, v. 87, p. 901–908, doi:10.1306/01290300181.

Silvestro, J., and Atencio, M., 2009, La cuenca cenozoica del Río Grande y Palauco: Edad, evolución y control estructural, faja plegada de Malargüe: Revista de la Asociación Geológica Argentina, v. 65, p. 154–169.

Stacey, J.S., and Kramers, J.D., 1975, Approximation of terrestrial lead isotope evolution by a two-stage model: Earth and Planetary Science Letters, v. 26, p. 207–221, doi:10.1016/0012-821X(75)90088-6.

Tibaldi, A., 2005, Volcanism in compressional tectonic settings: Is it possible?: Geophysical Research Letters, v. 32, L06309, doi:10.1029/2004GL021798.

Tibaldi, A., 2008, Contractional tectonics and magma paths in volcanoes: Journal of Volcanology and Geothermal Research, v. 176, p. 291–301, doi:10.1016/j.jvolgeores.2008.04.008.

Tibaldi, A., Corazzato, C., and Rovida, A., 2009, Miocene–Quaternary structural evolution of the Uyuni-Atacama

region, Andes of Chile and Bolivia: Tectonophysics, v. 471, p. 114–135, doi:10.1016/j.tecto.2008.09.011.

Tibaldi, A., Bonali, F.L., and Corazzato, C., 2014, The diverging volcanic rift system: Tectonophysics, v. 611, p. 94–113, doi:10.1016/j.tecto.2013.11.023.

Tunik, M., Folguera, A., Naipauer, M., Pimentel, M., and Ramos, V.A., 2010, Early uplift and orogenic deformation in the Neuquén Basin: Constraints on the Andean uplift from U-Pb and Hf isotopic data of detrital zircons: Tectonophysics, v. 489, p. 258–273, doi:10.1016/j.tecto.2010.04.017.

Turienzo, M., Sánchez, N., Dimieri, L., Lebinson, F., and Araujo, V., 2014, Tectonic repetitions of the Early Cretaceous Agrio Formation in the Chos Malal fold-and-thrust belt, Neuquén Basin, Argentina: Geometry, kinematics and structural implications for Andean building: Journal of South American Earth Sciences, v. 53, p. 1–19, doi:10.1016/j.jsames.2014.04.004.

Uliana, M.A., and Legarreta, L., 1993, Hydrocarbons habitat in a Triassic-to-Cretaceous Sub-Andean setting: Neuquén Basin, Argentina: Journal of Petroleum Geology, v. 16, p. 397–420, doi:10.1111/j.1747-5457.1993.tb00350.x.

Valentine, G.A., and Krogh, K.E.C., 2006, Emplacement of shallow dikes and sills beneath a small basaltic volcanic center—The role of pre-existing structure (Paiute Ridge, southern Nevada, USA): Earth and Planetary Science Letters, v. 246, p. 217–230, doi:10.1016/j.epsl.2006.04.031.

Veiga, G.D., Spalletti, L.A., and Flint, S., 2002, Aeolian/fluvial interactions and high-resolution sequence stratigraphy of a non-marine lowstand wedge: The Avilé Member of the Agrio Formation (Lower Cretaceous), central Neuquén Basin, Argentina: Sedimentology, v. 49, p. 1001–1019, doi:10.1046/j.1365-3091.2002.00487.x.

Vergani, G.D., Tankard, A.J., Belotti, H.J., and Welsink, H.J., 1995, Tectonic evolution and paleogeography of the Neuquén Basin, Argentina, *in* Tankard, A.J., Suárez, R., and Welsink, H.J., eds., Petroleum Basins of South America: American Association of Petroleum Geology Memoir 62, p. 383–402.

Watanabe, T., Koyaguchi, T., and Seno, T., 1999, Tectonic stress controls on ascent and emplacement of magmas: Journal of Volcanology and Geothermal Research, v. 91, p. 65–78, doi:10.1016/S0377-0273(99)00054-2.

Weaver, C.E., 1931, Paleontology of the Jurassic and Cretaceous of West Central Argentina: Seattle, Washington, University of Washington Press, 594 p.

Zamora Valcarce, G., Zapata, T.R., del Pino, D., and Ansa, A., 2006, Structural evolution and magmatic characteristics of the Agrio fold-and-thrust belt, *in* Kay, S.M., and Ramos, V., eds., Evolution of an Andean Margin: A Tectonic and Magmatic View from the Andes to the Neuquén Basin (35°–39°S Lat.): Geological Society of America Special Paper 407, p. 125–145.

Zöllner, W., and Amos, A.J., 1973, Descripción Geológica de la Hoja 32b, Chos Malal (Prov. Neuquén): Instituto de Geología y Recursos Minerales–El Servicio Geológico Minero Argentino Boletín 143, scale 1:200000.

Science Editor: David Ian Schofield
Associate Editor: Jean Bédard

Manuscript Received 30 April 2015
Revised Manuscript Received 16 June 2015
Manuscript Accepted 22 July 2015

Printed in the USA

Geological Society of America Bulletin

Structure and evolution of volcanic plumbing systems in fold-and-thrust belts: A case study of the Cerro Negro de Tricao Malal, Neuquén Province, Argentina

Derya Gürer, Olivier Galland, Fernando Corfu, Héctor A. Leanza and Caroline Sassier

Geological Society of America Bulletin published online 2 September 2015;
doi: 10.1130/B31341.1

Notes